TUNABLE DIODE LASER ABSORPTION SPECTROSCOPY VERIFICATION ANALYSIS FOR USE IN THE COMBUSTION OPTIMIZATION AND ANALYSIS LASER LABORATORY

THESIS

Christina R Serianne

AFIT/GAE/ENY/09-M17

DEPARTMENT OF THE AIR FORCE

AIR UNIVERSITY

AIR FORCE INSTITUTE OF TECHNOLOGY

Wright-Patterson Air Force Base, Ohio

The views expressed in this thesis are those of the author and do not reflect the official policy or position of the United States Air Force, Department of Defense, or the United States Government.

AFIT/GAE/ENY/09-M17

TUNABLE DIODE LASER ABSORPTION SPECTROSCOPY VERIFICATION ANALYSIS FOR USE IN THE COMBUSTION OPTIMIZATION AND ANALYSIS LASER LABORATORY

THESIS

Presented to the Faculty

Department of Aeronautics and Astronautics

Graduate School of Engineering and Management

Air Force Institute of Technology

Air University

Air Education and Training Command

In Partial Fulfillment of the Requirements for the

Degree of Master of Science in Aeronautical Engineering

Christina R Serianne, BS

Civilian

March 2009

AFIT/GAE/ENY/09-M17

TUNABLE DIODE LASER ABSORPTION SPECTROSCOPY VERIFICATION ANALYSIS FOR USE IN THE COMBUSTION OPTIMIZATION AND ANALYSIS LASER LABORATORY

Christina R. Serianne, BS

Civilian

Approved:

_____/signed/_____ _____

LtCol Richard Branam, USAF (Chairman) date

_____/signed/_____ _____

Dr. Paul King (Member) date

_____/signed/_____ _____

Dr. Mark Reeder (Member) date

AFIT/GAE/ENY/09-M17

Abstract

The AFIT Combustion Optimization and Analysis Laser (COAL) laboratory has state-of-the-art laser diagnostic capability for combustion process. The research for this thesis served to enhance the COAL lab's capability. Currently, there are no known commercially available tunable diode lasers that produce Ultra-Violet radiation required for this analysis. Sum-frequency generation at 313.5 nm was utilized for high speed OH absorption and temperature measurements at a rate of 2 kHz. The Tunable Diode Laser Absorption Spectroscopy system was validated by comparison with theoretical and well characterized experimental data by operating the system over a wide range of conditions for an H_2 laminar flame produced by a Hencken burner. The TDLAS system was able to perform at reasonable accuracy. After validation, the system was also characterized for a turbulent environment by comparing turbulent and flame structure theory with results obtained from a C_2H_4/N_2 jet flame. The testing was also conducted for a range of conditions and produced reasonable results. The accuracy of the system is sufficient for utilization in investigating behavior in a turbulent, combusting environment.

Acknowledgements

I would first like to thank my family, especially my daughter. She has sacrificed more than anyone for me to complete the required coursework and thesis. I am so proud and grateful to have such a wonderful daughter and for all your encouragement and support. I am humbled by your undying faith in me and believing that "Mommy can do anything". You're the best kid ever! Thanks to my parents for always being there for me and supporting me through all my endeavors. I couldn't have asked for better parents.

My undying gratitude to Lt. Col. Richard Branam for all your support, faith, and guidance along the way. You are an amazing instructor, mentor, and advisor. Thank you for believing in me when I didn't believe in myself.

Many thanks to Stan Kostka and John Hixenbaugh for the knowledge and guidance in the COAL Lab. The many enlightening lunches and long hours taught me volumes about lasers and life in general. You guys are the best!

Most thanks of all goes to Jesus Christ, my Lord and Savior. Thank you for giving me the talent to be able to complete this challenge set before me. I know with you, all things are possible.

Table of Contents

Page

Page

Page

List of Figures

Page

Page

Page

List of Tables

Page

List of Symbols

Symbol	
a	Moles of air, coefficient of stoichiometry, Voigt parameter
A	Area
atm	pressure measurement units (atmosphere)
A/F	Air-to-fuel ratio
c_A	Species concentration
c	Speed of light (m/s)
cm	Centimeters
CO	Carbon Monoxide
CO_2	Carbon Dioxide
C_p	Constant-pressure specific heat
C_xH_y	General formula of a hydrocarbon
CH_4	Methane
C_2H_4	Ethylene
D	Diameter
DC	Direct current
g	Multiples of the gravitational constant
$g(\nu)$	Voigt profile line shape function
$g_C(\nu)$	Pressure broadening profile line shape function
$g_D(\nu)$	Doppler profile line shape function
hr	Hour
H_C	Heat of combustion of fuel
Hz	Hertz
H_2	Hydrogen

H_2O	Water
I	Absorption sample transmission intensity
I_o	Incident laser light intensity
J	Joules
k	Boltzman's constant: $1.38065 \times 10^{-23} \frac{m^2 kg}{s^2 K}$
k_v	Absorption coefficient
K	Degrees Kelvin
kg	Kilograms
kJ	Kilojoules
l	Absorption path length
m, m	Mass, meter
$\dot{m}$	Mass flow rate
mJ	Millijoules
mm	Millimeters
ms	Millisecond
m/s	Meters per second
mW	Milliwatt
min	minute
MW	Molecular Weight (kg/kg mole)
Nd^{3+}	Neodymium ions
nm	Nanometer
ns	Nanosecond
N_2	Nitrogen
NO_X	Oxides of Nitrogen
OH	Hydroxyl
O_2	Oxygen
P	Pressure (atm, psi)
$P(U)$	Probability density function

Q	Heat
R	Intensity ratio
R_e	Reynolds number
s, s	Entropy, second
S_B	Buoyant flame speed
S_L	Laminar flame speed
S_T	Turbulent flame speed
SLPM	Standard liters per minute
T	Temperature (K)
T.I.	Turbulent intensity
U	Combustor inlet velocity (m/s), quantity of interest in turbulence
V,v	Velocity (m/s)
$\dot{V}$	Volumetric flow rate (scf/m)
x	Number of carbon atoms, Voigt parameter
y	Number of hydrogen atoms
Y_3VO_4	Crystalline orthovanadate
(A-X)	OH energy states
Å	Angstroms
$\frac{dP}{P}$	Pressure drop
β, γ	Exponents for laminar flame speed calculation
ε/κ	Quenching temperature factor
ϕ	Equivalence Ratio
η_b	Combustion efficiency
Ω	Ohms
ρ	Density
τ	Finite time
μ	Dynamic viscosity

ν_o	Transition center frequency
$\Delta \nu_c$	Frequency spread
$\Delta \nu_D$	Transition width
σ	Standard deviation

List of Abbreviations

Abbreviation	
AFIT	Air Force Institute of Technology
AFRL	Air Force Research Laboratory
CARS	Coherent anti-Stokes Raman-Scattering
CEA	Chemical equilibrium with calculations software
CFD	Computational Fluid Dynamics
CIAC	Cavity-in-a-cavity
COAL	Combustion Optimization and Analysis Laser
CT	Constant-temperature
CTB	Continuous turbine burner
DFB	Distributed Feedback Laser
EI	Emission Index
FWHM	Full-width, half-maximum
HPT	High-pressure turbine
IHPTET	Integrated High Performance Turbine Engine Technology
ITB	Inter-stage turbine burner
LBO	Lean Blowout
LDV	Laser Doppler Velocimetry
LHV	Lower heating value
LII	Laser-induced incandescence
LIF	Laser induced flourescence
LPT	Low-pressure turbine
MATLAB	Material Laboratory computer programming language
NASA	National Aeronautics and Space Administration

Nd:YAG	Neodymium-doped yttrium aluminium garnet
Nd:YVO_4	Neodymium-doped yttrium orthovanadate
PDE	Pulsed Detonation Engine
PDF	Probability Density Funciton
PIV	Particle Imaging Velocimetry
PLIF	Planar Laser Induced Fluorescence
ROI	Region of interest
RVC	Radial Vane Cavity
SAE	Society of Automotive Engineers
ST	Specific thrust
TDLAS	Tunable Diode Laser Absorption Spectroscopy
TSFC	Thrust specific fuel consumption
TVC	Trapped Vortex Combustion
UCC	Ultra Compact Combustor
UHC	Unburned hydrocarbons
UV	Ultra-violet
VI	Virtual Instrument
2-D	Two dimensional

TUNABLE DIODE LASER ABSORPTION SPECTROSCOPY VERIFICATION ANALYSIS FOR USE IN THE COMBUSTION OPTIMIZATION AND ANALYSIS LASER LABORATORY

1 Introduction

1.1 Research and Design Perspective

The United States is one of the world's largest consumers of oil per capita[1]. A significant reason for the United States oil consumption rate is that it is utilized for fuel in the transportation industry, with aviation fuel being the third highest product in demand [1]. Commercial and private fuel consumption in most industries has decreased due to the ever increasing prices of fuel, with no relief in sight. However, the United States armed forces do not possess the luxury of simply cutting back on operations. With the ever present and evolving threats to our national sovereignty, the military must keep abreast with training and missions, no matter the cost. Furthermore, environmental concerns and responsibilities must also be a considered in the preservation our Great Nation. With this in mind, improving fuel efficiencies, speeds, endurance, altitudes, and payloads are at the forefront of developmental sciences for existing and new aircraft. These considerations lay the foundation of exciting research in combustion technologies. Improving upon existing combustion methods would decrease thrust-specific fuel consumption and increase thrust to weight ratios, which directly translates into lower operational costs. In order for this progress to be realized, it is essential that current and future propulsion research be directed toward highly efficient combustion processes.

A significant research effort has been embarked upon by the Air Force Institute of Technology (AFIT) and the Air Force Research Laboratory (AFRL). This effort focuses

on improving propulsion efficiency by employing several theories into one combustor. This combustion technology, called the Ultra Compact Combustor (UCC), implores replacing the traditional combustion section of a turbine engine with a circumferential burner which encircles the turbine section. The configuration permits the turbine section of the engine to fall directly aft of the compressor. Furthermore, the design of the actual combustor section permits for more efficient and complete burning of fuel, thereby increasing the thrust to weight ratio, efficiency, and fewer emissions of environmentally harmful substances.

Computational Fluid Dynamics (CFD) simulations of the UCC flow characteristics have been performed and documented.[2] Results from the CFD studies indicate great promise for significant improvements in propulsive efficiencies. More recent research efforts have been initiated to experimentally validate the theoretical results. The focus in AFIT's Combustion Optimization and Analysis Laser (COAL) Laboratory is to utilize various laser diagnostic techniques for interrogation of a small scaled version of the UCC.

1.2 VAATE

The Versatile Affordable Advanced Turbine Engine (VAATE) program is a successor to the hugely successful Integrated High Performance Turbine Engine Technologies (IHPTET) initiative implemented in the late 1980's by a multi agency governmental team, academia, and industry.[3] As a program, IHPTET performed exceptionally well in advancing turbine engine technologies by focusing on improving

thrust-to-weight ratios, reducing fuels consumption, and cutting production and maintenance costs. VAATE will share these same goals while adding durability and sustainability as vital criteria. Furthermore, VAATE is intent on a 10 fold increase in affordability by the year 2017.[3]

In order to meet the goal set forth by VAATE, AFRL Combustion Science Branch supports the research and development of inventive propulsive and combustion concepts. These concepts include: Trapped Vortex Combustion (TVC), Inter-Turbine Burner (ITB), Ultra-Compact Combustor (UCC), and Pulsed-Detonation Engines (PDE). Exploration of these innovative concepts are currently being accomplished through efforts in optical diagnostics, simulation and modeling, fundamental studies of aircraft fuels and their combustion, and development of progressive pioneering hardware [4.] The structure for the Combustion Science Branch program is illustrated in Figure 1.

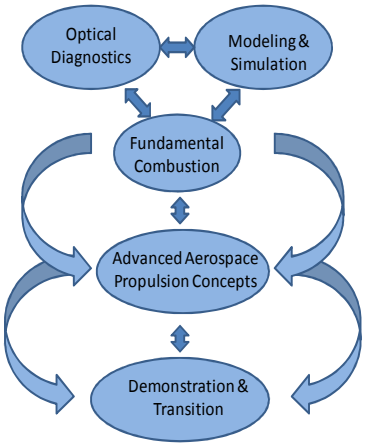

Figure 1: Combustion Sciences Branch Program Structure [4]

In order to support the VAATE initiative, this research focuses on the optical diagnostics of the turbulent flow characteristics. Such diagnostic techniques will then be applied to investigating the UCC.

1.3 AFIT COAL Laboratory Laser Diagnostic Systems

The various laser diagnostic systems in the AFIT COAL lab create a state-of-the-art combustion diagnostic environment. To illustrate the ability, a sample of the facility's inventory consists of several lasers, a variety of optics, lenses, and electronically controlled traverse systems on rails for high accuracy in alignment and data collection. Further expansion and upgrades to the inventory are ongoing enhancing the COAL lab capability and function.

The current laser diagnostic capabilities are the Particle Image Velocimetry (PIV) , Planar Laser Induced Fluorescence (PLIF) , Coherent Anti-Stokes Raman Scattering (CARS), Instantaneous Raman Scattering, Raman Spectroscopy, Laser Induced Incandescence (LII), and Tunable Diode-Laser-Based Absorption Spectroscopy (TDLAS).

The critical laser components that enable the application of these various interrogation techniques consist of: the Quanta-Ray PIV-Series dual pulsed Nd:YAG produced by Spectra-Physics, the Continuum ND6000 narrowband dye laser with a frequency doubler assembled by Innovative Scientific Solutions, Inc (ISSI), a broadband dye laser also assembled by ISSI, the Verdi 5 Nd:YVO_4 laser produced by Coherent, and

the DFB diode Laser produced by Cheetah. These laser systems are mounted on optics tables in the AFIT COAL laboratory.

Figures 2 through 5 show the various lasers currently in use as measurement devices for research in the AFIT COAL laboratory.

Figure 2: Quanta-Ray PIV-Series dual pulsed Nd:YAG laser

Figure 3: ND6000 narrowband dye laser with frequency doubler

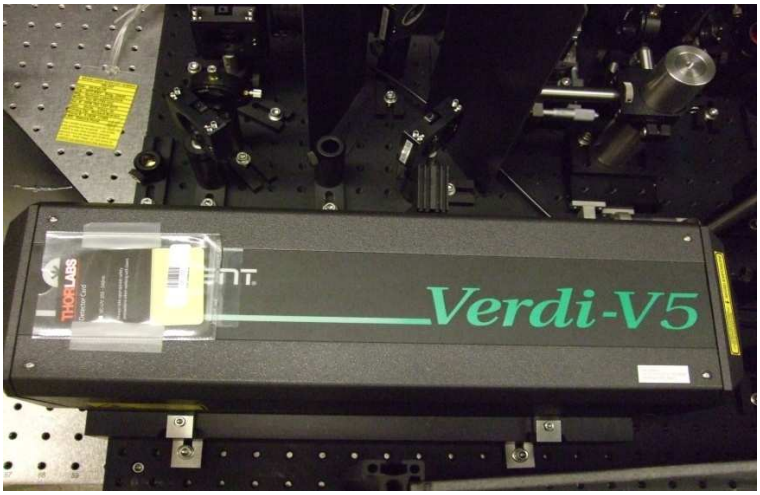

Figure 4: Coherent Verdi-5 Nd:YAG laser

Figure 5: Cheetah Series DFB diode laser

1.4 Objectives

Research being performed cohesively by AFRL and AFIT for the UCC consists of three main goals. The first being to explore the effects of body forces upon the

combustion process in an actual UCC design. It has been found that the turbulent Reynolds number in the main flow decreases as the mass flow to the cavity increases. This research endeavor by AFRL and AFIT is to ascertain if body forces cause this behavior or if it is a result of flow shear. Holding velocity constant while varying the radius of curvature and thus the circumferential force (g-load) will prove useful in achieving the objective. Effects of varying air jet geometry, equivalence ratios, and main airflow velocity will also be probed in further experimentation beyond this thesis. The second goal is to investigate Trapped Vortex combustion efficiencies in the UCC. The optimal environment for extracting mass from the cavity into the main flow can be discovered by utilizing experimental data that supports CFD model results. Effects on performance and range of operation by trapping a vortex in the cavity will be investigated as well. The third and final goal is to examine and comprehend the interaction between the cavity and the vane cavity. This is crucial to ensure optimum mass transfer from the cavity to the main flow. Geometrical variations of the radial vanes and the RVC and their effects on the UCC performance parameters will be accomplished through CFD studies. Optimal geometries discovered through CFD assessment will provide the foundation for experimental models.

The focus of this research will be on adding to the body of knowledge for the first and second UCC research goals. Implementing a time-accurate combustion diagnostic tool is essential in pursuing turbulence statistics and influences in the flow field. The diagnostic will be developed to investigate body forces in a turbulent flame in support of

the UCC. Data will be captured and analyzed in both a steady premixed flame as well as an unsteady, turbulent flame. This research will be conducted in AFIT's Combustion Optimization and Analysis Laser (COAL) Laboratory. The investigation and diagnostic technique to be utilized is Tunable Diode-Laser-Based Absorption Spectroscopy (TDLAS).

Prior to commencement of testing, the laser based diagnostic system was built, laser aligned, and operational functioning verified by the researcher and contractor Stan Kostka. This was the basis of the first objective of this thesis. Functionality will be verified by passing the laser through a well characterized laminar flame and analyzing the results. The laminar flame will be a hydrogen-air flame produced by a Hencken burner, shown in Figure 6.

Figure 6: Laminar Hydrogen-air flame from Hencken burner

Recommendation was given in reference 5 to operate the Hencken burner at higher flow rates than previously research so as to prevent heat transfer to the device by lifting the flame from the burner's surface [5.] This recommendation was followed for research completed in reference 6 and will also be implemented in this study[6]. This calibration will serve as verification of the TDLAS system's ability to detect the hydroxyl radical (OH).

The second objective is to develop the TDLAS system to investigate body forces in a turbulent flame was pursued by analyzing body forces in their natural turbulent state. The turbulent flame was produced from a premixed jet diffusion burner. The results provide a foundation for the analysis technique utilizing the TDLAS system for interrogating of a region of interest in the UCC.

The final objective is to capture unsteady flame characteristics. By characterizing a turbulent flame with established statistics, this gives a better understanding of expected behavior in the UCC. This will be accomplished by passing the laser through a turbulent jet flame and analyzing the resulting data. In order to truly capture the turbulent behavior, the laser will be traversed from the center of the jet flame to the edge with resulting data providing a map of the jet flame.

2 Theory and Background

2.1 Combustion

Merriam-Webster Dictionary defines combustion in three ways: "*an act or instance of burning; a usually rapid chemical process that produces heat and usually light; violent agitation*". The definition that most applies to this research is that concerning rapid chemical processes. This concept is intuitive as combustion in an aircraft engine is indeed an expeditious chemical reaction of a fuel and an oxidizer so as to produce a flame (heat and light) providing the medium for propulsion of the aircraft. Moreover, this definition gives the inherent significance of the chemical reaction process in combustion [7].

To investigate the significance of the chemical reaction, we must first consider exactly what is involved in the chemical reaction for combustion. It has been established that combustion is indeed a complex sequence of chemical reactions between a fuel and an oxidizer. In general, the resulting product is a flame or a glow (heat and light). However, there is a considerable amount of chemistry occurring as well as other very important mechanisms that require consideration when designing a combustion device. Discussion of combustion from here forth will be relative to the explanation and understanding of combustion in an air vehicle utilizing a hydrocarbon fuel, unless specified otherwise.

2.1.1 Complete Combustion

To get a thorough understanding of what is meant by the chemical process by which combustion occurs, a brief overview of some basic principles of the combustion process will be addressed. Complete combustion of a hydrocarbon fuel is a chemical reaction in which oxygen and a fuel combine and the only products are carbon dioxide (CO_2), water vapor (H_2O), and energy in the form of heat. A simplified illustration of this is the chemical reaction equation for the combustion of methane (CH_4) and oxygen (O_2).

$$CH_4 + 2O_2 \rightarrow 2H_2O + CO_2 \tag{1}$$

However, in most combustion devices, the oxidizer is ambient air. Since the most abundant element in air is nitrogen (N_2), this must be taken into consideration when using air as the oxidizer. Therefore, equation (1) becomes

$$CH_4 + 2O_2 + 7.52N_2 \longrightarrow 2H_2O + CO_2 + 7.52N_2 \tag{2}$$

Though ideal, complete combustion almost never occurs. There are typically some unburned hydrocarbons as well as other byproducts in the exhaust gases from the combustion process depending on actual mixture concentrations as well as many other factors. These other byproducts are typically in the form of carbon and hydrogen compounds as well as nitrogen oxides (NO_x). In the combustion process, stable species are joined by radicals as well as the intermediate species, such as hydroxyl (OH), often shown where the combustion process is most vigorous. For this reason, researchers often

use this radical as the flame location marker. Hydrocarbon combustion has historically had issues with producing NO_x , which is a harmful and relatively slow process. The kinetics and combustion models highlight the importance of evaluating and minimizing the amount of such compounds produced.

2.1.2 Stoichiometric Relationship

Stoichiometry is used for determining mixture concentrations in chemical reactions based upon the law of conservation of mass. When applying this principle to combustion, an ideal stoichiometric mixture means the exact amount of oxidizer needed to completely combust a specific amount of fuel is available. Should there be more than the stoichiometric amount of oxidizer needed for complete combustion, the oxidizer-fuel mixture is said to be fuel lean. If there is less than the stoichiometric amount of oxidizer required, then the mixture is said to be fuel rich [7].

The following equation shows how a stoichiometric relationship for a hydrocarbon fuel can be determined:

$$C_x H_y + a(O_2 + 3.76N_2) \longrightarrow xCO_2 + \left(\frac{y}{2}\right)H_2O + 3.76aN_2 \tag{3}$$

where

$$a = x + \frac{y}{4} \tag{4}$$

By utilizing equations 3 and 4, the following relationship can be established as the stoichiometric air-fuel ratio:

$$(A/F)_{ST} = \frac{4.76a}{1}\frac{MW_{air}}{MW_{fuel}} \quad (5)$$

where MW_{air} and MW_{fuel} are the molecular weights of the air and fuel, respectively.[7] This relationship is employed to help establish operating conditions for this research.

2.1.3 Equivalence Ratio

The equivalence ratio (ϕ) provides a quantitative assessment of the air-fuel mixture as

$$\phi = \frac{(A/F)_{ST}}{(A/F)_{ACTUAL}} = \frac{(F/A)}{(F/A)_{ST}} \quad (6)$$

From equation 6, values of $\phi > 1$ are fuel rich mixtures, and fuel lean for values of $\phi < 1$. For a stoichiometric mixture, $\phi = 1$.

2.1.4 Flame Speed and Flame Stability

Flame speed is an important concept in combustion, but one must be careful to distinguish exactly what type of flame speed is being discussed. Laminar flame speed is defined as the velocity at which a flame front moves through a combusting medium. Laminar flame speed (S_L) is a function of temperature, pressure, equivalence ratio and composition of the reactants. There are several correlations to determine flames speed, with a relatively reliable relationship given by

$$S_L = S_{L,ref}\left(\frac{T_u}{T_{u,ref}}\right)^{\gamma}\left(\frac{P}{P_{ref}}\right)^{\beta}\left(1-2.1Y_{dil}\right) \qquad (7)$$

where $T_{u,ref}$ and P_{ref} are reference temperature of 298 K and pressure of 1.0 atm, respectively. Furthermore, $S_{L,ref}$ is a reference flame speed found at room temperature. The exponents of γ and β are functions of ϕ.[7]

Turbulent flame speed (S_T) is a mass consumption rate per unit area divided by the density of the unburned reactant mixture. The clear distinction here is that S_L is a chemical kinetic property of the unburned reactant mixture that can be assigned, whereas S_T is dependent upon properties of the turbulent flow field in which it resides.[8]

As long as the reactant mixture remains at a constant flow rate for a laminar flame, it is very stable. However, stability for a turbulent flame is dependent upon the flow environment. This creates challenges in actual combusting devices as flame stability becomes a real concern. Flame stabilization occurs when flow velocity out and burning back are equal, or when a flame is attached.[7] A flame is considered attached if the flow rate is such that the base of the jet flame resides extremely close to the burner tube outlet. As the flow rate increases, voids form in the flame near the base creating a situation where there is no continuous flame near the burner outlet. This is known as liftoff. Continued significant increases in flow rate result in blowout. This is where the velocity of the incoming reactant mixture exceeds that of the flame [7].

Stability of flame is clearly a very important issue. Since it is not possible to consistently hold the velocity of the incoming reactant mixture below the flame speed, a

technology referred to as flame holding was developed. Flame holding is a technique where by a small obstruction is placed in the flow field thereby creating a stagnant area for stationary location of a portion of the flame. The stationary flame then propagates into the reactant mixture as it passes. This maintains combustion in a flow field that is moving faster than the flame speed. This technique is necessary for the small-scale UCC ignition device, as the flow rate required to create the necessary flame length exceeds that of the flame speed.

2.2 Combustion Performance Parameters

To provide an assessment of all combustion devices relative to one another, there is a set of parameters commonly used for most devices. Four of the most widely used parameters when discussing combustion as it related to aircraft engines are: combustion efficiency, pressure loss, thrust specific fuel consumption, and specific thrust. With increasing attention to environmental concerns, emissions index is also a significant consideration in performance. For a complete overview of all combustion performance parameters, the author directs the reader to the text *Gas Turbine Combustion*, by Arthur H. Lefebvre and *An Introduction to Combustion*, by Stephen R. Turns.

2.2.1 Combustion Efficiency

Combustion efficiency (η_b) is a ratio of actual performance to ideal performance of the combustor in terms of the completeness of combustion. Combustor efficiency is defined as

$$\eta_b = \frac{1}{\dot{m}_f h}\left[\left(\dot{m}_{air} + \dot{m}_f\right)C_{p_{out}}T_{out} - \dot{m}C_{p_{in}}T_{in}\right] \quad (8)$$

Where $\dot{m}_f$ and $\dot{m}_{air}$ are the fuel and air mass flow rates respectively, ($C_{p_{out}}T_{out}$) is the stagnation enthalpy leaving the combustor, and ($C_{p_{in}}T_{in}$) is the stagnation enthalpy entering the combustor [9].

2.2.2 Pressure Loss

Pressure loss is a critical performance parameter and is a resultant of hot and cold losses in a combustor. Hot pressure losses are due to the actual combustion process and acceleration of the flow. Cold losses are a result of friction and turbulence along the combustor walls. Taking all factors into account, pressure loss can be calculated as:

$$\frac{dP}{P} = 100 * \frac{P_3 - P_4}{P_3} \quad (8)$$

P_3 and P_4 are the stagnation inlet and exit pressure, respectively[6].

2.2.3 Thrust Specific Fuel Consumption

Thrust Specific Fuel Consumption (TSFC) is the ratio of the mass fuel flow rate to the amount of thrust produced by the engine. This can be shown mathematically as

$$TSFC = \frac{\dot{m}_f}{T} \quad (9)$$

Where $\dot{m}_f$ is the fuel mass flow rate and T is thrust. As is evident, fuel flow rate

and thrust are two very important factors. The amount of thrust is critical to actual flight. However, a key performance factor is to consider how much fuel it takes to produce the desired thrust. With this consideration, lower values of the TSFC indicate better performance.[9]

2.2.4 Specific Thrust

Specific Thrust (ST) is the ratio of thrust to the free stream mass flow rate.

$$ST = \frac{T}{\dot{m}_{air}} \tag{10}$$

Where T is thrust and $\dot{m}_{air}$ is the free stream mass flow rate. Though it is known thrust is an important parameter for engine performance, so too is the free stream mass flow rate. The parameter, ST, permits that analysis of how much thrust an engine can produce from a fixed mass flow rate of air. As one can infer from equation 10, as the value of ST increases, so too does the performance of the engine.[9]

2.2.5 Emissions Index

Monitoring the concentrations of environmental pollutants emitted is critical. A metric utilized by the Society of Automotive Engineers (SAE) for such a measurement is the Emissions Index (EI). EI is used to calculate the amount of pollutants emitted per quantity of fuel used. SAE has established a widely accepted method for calculating EI in an aerosol hydrocarbon fuel. This simple algebraic method can be shown as

$$EI_z = \left(\frac{mol_z}{mol_f}\right)\left(\frac{M_z}{M_f}\right)(1000) \tag{11}$$

Where subscript z is any species of interest, mol_z and mol_f are the molar concentration of the species of interest and the fuel respectively. M_z and M_f are the molecular weight of the species of interest and fuel respectively[10].

2.3 Conventional Combustors

A conventional jet engine consists of an inlet, compressor section, combustor, turbine section, and exhaust nozzle. Figure 7 depicts a conventional combustor. The combustion section comprises a considerable portion of the conventional jet engine.

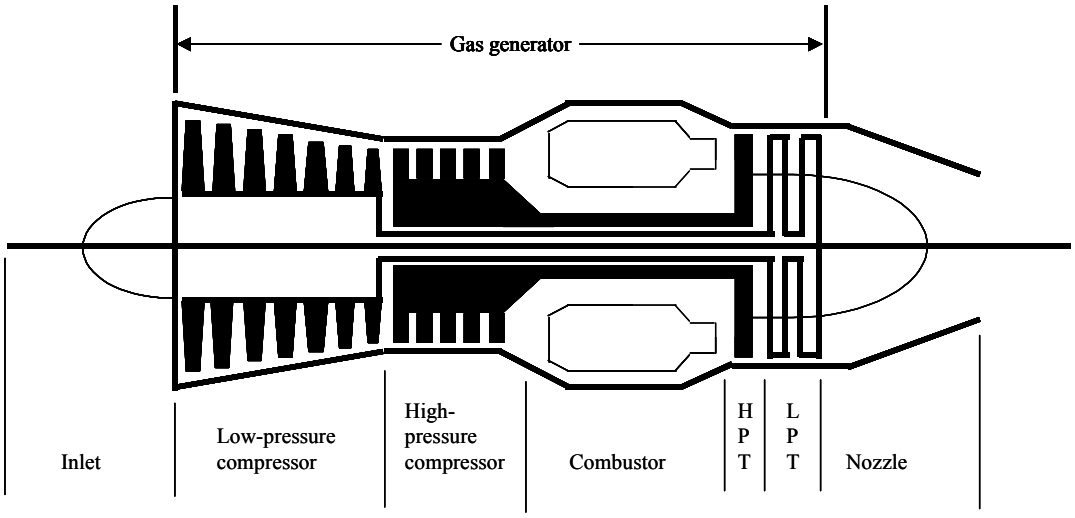

Figure 7: Schematic of a turbojet with dual axial compressor and turbine [11]

Operation of a traditional combustor occurs by spraying fuel into incoming hot air. This is the flame-stabilized region. As the fuel droplets evaporate and mix with the

air, the fuel-air mixture is ignited. This fuel rich gas is mixed with cooling air by axially passing it through an area with cooling holes in the combustion liner. This process is shown in Figure 8.

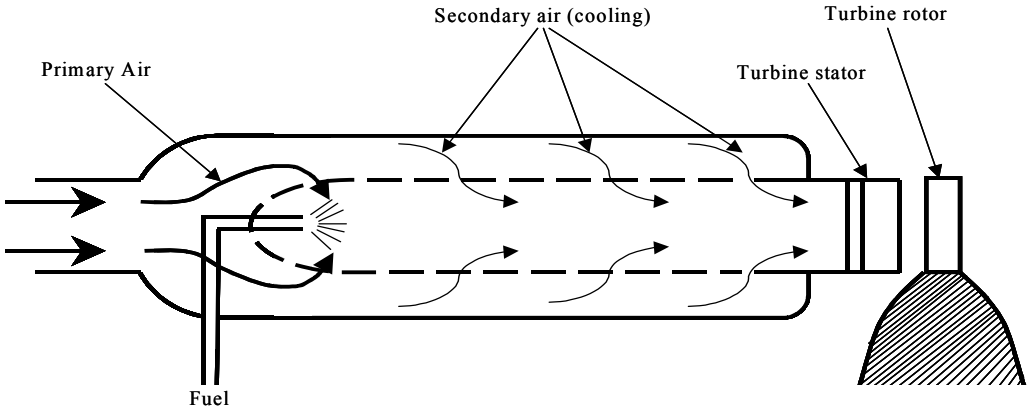

Figure 8: Flow through standard combustor [11]

A good combustor design is considered one in which complete combustion is accomplished with minimal pressure loss, there exists uniform temperature distributions eliminating hot spots, the combustion is stable, and all this occurs in as minimal an area as possible.[9]

2.4 The Ultra Compact Combustor (UCC)

The combustor design currently used in most aircraft is one in which a swirl mechanism is utilized to increase efficiency. The swirl works by inducing a spin into the flow of the air in order to get a more complete mixture with the fuel as well as to stabilize the combustion process. This is of great importance as the more controlled the combustion, the more reliable the energy release is from the process. The purpose for chemically reacting processes is to convert the chemical energy into useful work. In this

conversion, time and space are both crucial and finite. The longer the swirling, combusting gases are permitted to remain in the combustor, the more complete the combustion. Residence time has to be balanced with increased engine weight. In order to maintain an overall system balance to maximize aircraft performance, designers constrain combustor length, accepting some inefficiencies in the combustion process. Research to improve upon currently used combustion technology proves paramount, then, to improvements in jet engines. Such research has produced the concept of the UCC. The UCC lessens the effects of the time and space constraints by lengthening the path and mechanism for combusting gases, directly increasing residence time, permitting a more efficient burn.

Two primary mechanisms that enable the improvements of combustors in the UCC are trapped vortex combustion (TVC) for flame stabilization and the application of centrifugal force to improve mixing. TVC is an enhanced version of the conventional swirl stabilized combustion, which utilizes the physics of vortex development in a cavity residing within the combustor. This approach has proven to be a much more effective method of flame stabilization with the added benefit of serving as a highly efficient combustion zone for the burner.[12] Figure 9 depicts a method using vortex shedding from the main flow into a cavity while also injecting cavity air to create the necessary vortex motion to sustain combustion. Research completed by Sturgess et al. found cavity airflow rates between 5%-10% of the main flow created the best environment for TVC.

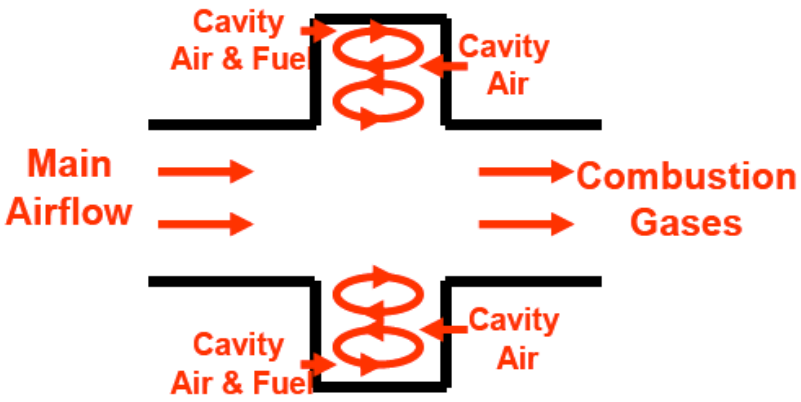

Figure 9: TVC utilizing main flow shed vortices for cavity combustion [13]

The idea for centrifugal force application was developed from studying and understanding the significance of buoyant forces in the combustion process. A centrifugal force can be introduced into a flow by rotating said flow at high velocities. The resulting centrifugal force field, known as a "g-load", improves mixing as well as increases the flame propagation rate approximately proportional to the square root of the applied g-load[14]. Prior to research of centrifugal force effects on combustion, researchers focused on two primary flame propagation means, laminar flame transport and turbulent flame transport. There was a third flame spreading mechanism explored, buoyant bubble transport. The flame speed in hydrocarbon-air mixtures of laminar flames is typically 0.3 m/s; 0.6 to 6 m/s for turbulent flames, and anywhere from 18 to 30 m/s for buoyant bubble flames. It was further exhibited buoyant bubble conditions fully exist in a flow with centrifugal loading from 500 g's and up to about 3500 g's, establishing an upper bound for the buoyant bubble flame propagation condition.[14]

By employing these mechanisms, the UCC exhibits significant physical differences from a conventional combustor. It is designed as a circumferential cavity around the axis of the engine. Fuel and air are injected into the UCC from the surrounding cavity. In the laboratory model, there is a recursive pattern of two air ports and one fuel port for a total of six fuel nozzles and 24 air ports. The air ports are situated at an induction angle of 45-degrees to create high velocity spinning inside the cavity. Such velocities provide a circumferential force ranging from 300-4000 g's, thereby inducing the buoyant bubble combustion. This results in a density gradient of the flow within the combustor. The less dense hot combustion products move toward the inside and are extracted into the main flow while the cold, denser unburned fuel and air mixture are pushed toward the outer wall. Flow pattern and basic design of the UCC appears below in Figure 10.

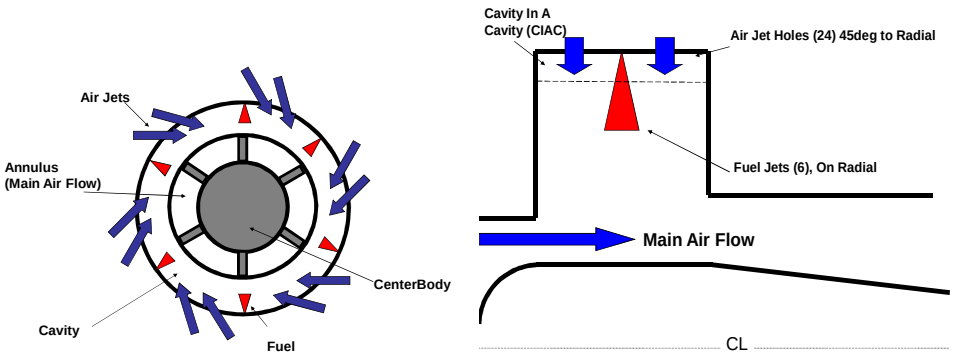

Figure 10: UCC major design features [15]

The UCC basic structure consists of a radial center body with six radial vanes supporting the circumferential cavity. Each of these vanes contains a built in radial-vane

cavity (RVC). The RVC's permit radial transport of the cavity fuel and air mixture to the main flow while also providing a medium for further combustion of the mixture[16]. This can be visualized in Figure 11 below.

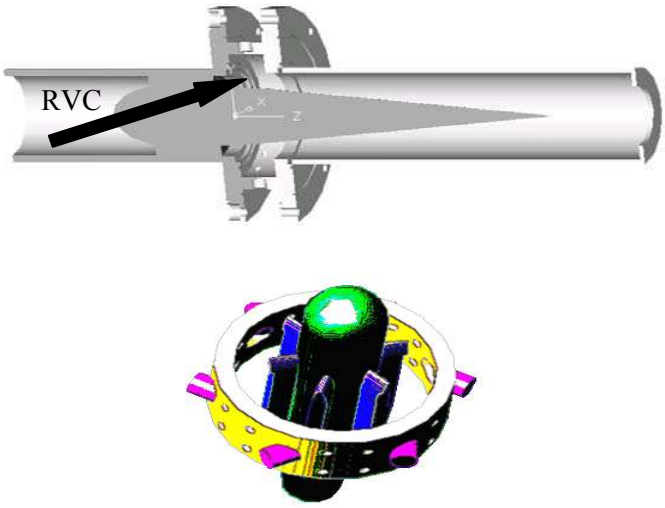

Figure 11: Basic UCC structure [16]

Previous testing shows the UCC will provide significant enhancements to currently implemented combustion technology. The physical size of the UCC is approximately 66% smaller than a traditional combustor while boasting efficiencies higher than 99% over a broad operating range. Indications are the UCC will improve thrust-to-weight ratios by up to 25% as well as increase specific thrust (ST) without increasing TSFC [17]

2.5 Previous Research

The basic concepts discussed previously have been explored in a myriad of manners. The research has proven to be very enlightening in the advancement of

combustion devices for jet engines, as well as highlighting areas needing further research. The following discusses some of this research.

2.5.1 Trapped Vortex Combustion

Trapped Vortex Combustion (TVC) provides flame stability. The TVC generates a vortex in an offset cavity from the main flow and holds the vortex in place. A properly chosen cavity size holds the vortex in place stably .[18]This fundamental research investigated how the TVC captured and transmitted non-reacting flows outside of a combustor configuration. A similar study was conducted with reacting flows finding similar results in a reacting vortex showing indeed a trapped flame in a cavity, serving as an effective stabilizer[19]. Further research found reacting flows maintained successful combustion when employing 5%-10% of main flow air injected directly into the cavity driving the vortex[12]. In the late 1990's, a TVC test rig was built and tested. Results for this TVC exceeded expectations. Over the traditional swirl stabilized combustor, the TVC boasted 50% improvement in lean blow out, 40%-60% improvement in NO_x emissions, and +99% combustion efficiency over a 40% wider operating range.[20]

2.5.2 Centrifugally Enhanced Combustion

A demonstration of significant increase in flame speed proportional to increased centrifugal force was also accomplished.[14] In this experiment, premixed fuel/air mixtures spun through a combustion centrifuge. The mixture was ignited and observed for flame behavior. It was noted that as the g-loading increased, so too did the flame speed, to a

point. Near 3500 g's, the flame speed made an abrupt reversal in upward trend. Further increase in g-loading created an environment where flame speed fell off in a steep linear fashion causing the flame to extinguish. This was an unexpected result, and suggested that there were flame speeds that exceeded the turbulent flame spreading limit of 6.0 m/s. With this research, flame speeds over 18 m/s were now being reported.[14] Clearly, there was an additional mechanism in place to facilitate such flame propagation rates. It was also found in addition to the two well know flame propagation regimes; laminar and turbulent; there was indeed a third mechanism in place. [14] The third flame speed enhancement was explained through bubble transport propagation and found the following relationship for buoyant flame speed (S_B):

$$S_B = 1.25\sqrt{g} \tag{8}$$

Further investigation of this high g-loading concept was incorporated by introducing a ring of inclined air injectors inducing swirling vortices in the combustor. The swirling vortices provide a solid explanation for the resulting increased combustion efficiencies.[21]

2.5.3 Inter-Stage Turbine Burning

The ideal Carnot cycle provides a theoretical upper limit for efficiency in constant temperature systems. Utilizing this concept, research performed at the University of California at Irvine has established the idea of a constant temperature (CT) gas turbine engine. System level analysis has shown increases in ST with little to no increase in TSFC. Systems based on CT designs are very promising, except this proposed process

requires burning to occur within the turbine rotor. The complexity of this problem is still limited by current technologies and material limits.[22] An alternative option is to employ an inter-stage turbine burner (ITB). The ITB concept is to burn fuel in the passages between stages within the turbine. Research has demonstrated a +50% increase in ST with no increase in TSFC, when adding a single stage ITB in a turbofan engine.[23]

2.5.4 Laser Diagnostics of Combustion

A myriad of laser based diagnostic techniques have been applied to reacting and non-reacting flows. These techniques provide highly accurate, rapid, non-intrusive measurements of varying flow characteristics such as combustion efficiency and radical concentration in the exhaust.[24]

The most commonly used techniques for measurements of OH and NO are absorption spectroscopy and Laser Induced Fluorescence (LIF).[25] Determining OH and NO emissions is extremely important as they give insight into the combustion process and efficiency of a given engine. OH is a good indicator of heat release and reaction zone for unsteady strain rate conditions and highly strained diffusion flames, respectively.[25] Detection of NO is crucial to measuring the amount released into the environment. When NO reacts with sunlight, the products are nitrogen oxides (NO_x) which adversely affect the environment. Combustion processes account for more than 95% of NO_x in the atmosphere. Over 95% of the combustion formed NO_x is initially in the form of NO. This being the case, a significant effort has been implemented to characterize and reduce the amount of NO from emissions.[26]

LIF is a valuable non-intrusive diagnostic technique focused on an area of interest. The basis for LIF comes from the emission and absorption of atomic spectra at high energy levels. Different photochemical processes excite radicals, moving them to higher energy states. These radicals are not comfortable in these higher energy states and naturally try to return to the lower energy state. When the radical shifts its energy state, photons are emitted from the upper energy level. The photon emission is indicated by light, or fluorescence. Several radicals are produced during combustion having high fluorescence times. As a specifically tuned laser is passed through the flow, the radicals will fluoresce with sufficient time to measure combustion location. The rate of the photon emission and wavelength of the photons is both concentration and temperature dependent. Comparing measured fluorescence with expected theoretical values provides temperatures and species concentrations.[27]

Absorption Spectroscopy is simpler than LIF and yet a very useful method for measuring combustion statistics, in terms of instrumentation and data evaluation. As a coherent beam is passed through a medium of interest, the absorption of a specific wavelength is recorded. Each species in the medium has very specific absorption characteristics, which can be related to concentration of that species through Beer's law.

$$I = I_o \exp\left(l \quad c_A k_\nu \right) \tag{9}$$

Where l is the path length of an absorption sample, c_A is the concentration of the absorbing species of interest, I_o is the incident intensity of the laser light source, I

is the intensity transmitted by the absorption sample, and k_ν is the frequency-dependant absorption coefficient. The concentration (c_A) is obtained by measuring the decrease of intensity between I_o and I through the use of Beer's law shown in equation 9. Capturing this information as the coherent light source is scanned over a specified wavelength range, temperatures can be inferred from the shape of the absorption information.[24]

2.5.5 UCC Research

A considerable amount of research in various areas has been performed for the Ultra Compact Combustor. The theory and application of the previously mentioned research methods have had a significant role in the development and understanding of the UCC.

As previously mentioned, TVC and centrifugally enhanced combustion have been combined as a basis for the design of the UCC. Implementation of both of these design features has give the UCC enhanced mixing and flame stabilization with increased flame speeds. This gives better performance over a conventional combustor in a much smaller package.

Utilizing the UCC as an ITB has been given much attention. As a conventional combustor is much too large to fit between turbine stages, the UCC is ideal given its compactness. As an ITB, the UCC would utilize swirl from the preceding turbine stage to drive the swirl in the cavity, thereby removing the need for a stator ahead of the

combustor. By removing the stator, this would further enhance the thrust-to-weight of the system.[28]

The UCC demonstrated efficiency increased and the observed flame length decreased by approximately 50% by increasing the g-load in the cavity. Furthermore, combustion efficiencies of > 99% were recorded.[15]

Investigation on the effects of fuel injector type and injection angle was conducted and results indicated a strong dependency of these properties on efficiency. Furthermore, pressure losses of no more than 2% were noted and validation of increased efficiency with increased g-loading was observed.[29] Pressure losses directly relate to system overall performance and thrust generating capability.

Laser Doppler Velocimetry (LDV) was utilized for measuring g-loading in the cavity at varying operating conditions. Tangential velocities of up to 45 m/s corresponded to g-loads of up to 4000g in the cavity. Combustion efficiency increased proportionally to the g-loading. The increased efficiency also suggests shorting residence time in the cavity of the combustor. The experimental results correlated well to the CFD study highlighting both combustion performance as well as operability of the UCC[28].

CFD has been an integral part of the development of the UCC. CFD studies have been conducted to theoretically predict flow characteristics within the UCC, as well as provide an understanding of combustor geometry influence on performance[5]. Other research implemented CFD codes investigating internal structure with an attempt to optimize key parameters.[13] The resulting CFD results compared well with existing

experimental data from a subscale UCC experiment run at AFRL. Further research continued this work by focusing more on the cavity-vane interaction inside the UCC sectional models.[2] The CFD resulted in key dimensions of the cavity vane as well as promoted the design employ a planar and curved sectional small-scale model of the UCC to further the investigation.[2]

UCC experiments began in 2007 with investigation of the 2-D planar, or infinite, radius of curvature model previously designed in reference 2.[5] This study utilized Planar Laser Induced Fluorescence (PLIF) diagnostic techniques. Results from this study also show a >99% efficiency for most operating conditions. The straight section provides a baseline for investigation of g-loading, as there was no curvature in the model. Of interest were experimental results for emissions were significantly different than those predicted by the CFD study.[5] The difference was attributed to error in the physical experiment such as fuel pooling and a low volume of emissions data collected. Hankins' experimental results as compared to theoretical CFD predictions appear below in Table 1.

Table 1: Hankins' experimental efficiency and emissions data compared with predictions of Moenter's CFD analysis.[5]

Condition	CO (ppm)	NO_x (ppm)	UHC (ppm)	% O_2	% CO_2	η_b (%)
EXP ATM1	1577.90	7.00	1740.00	18.84	2.08	99.88
CFD ATM1	2586.95	102.81	1.35	16.23	2.85	99.12
EXP ATM2	208.00	1.30	790.00	20.87	0.51	99.92
CFD ATM2	1665.53	42.43	0.72	16.01	3.05	99.45

Continued investigation of the 2-D planar model was conducted also using PLIF as the laser diagnostic technique. The laser was passed through a quartz window built

into the side of the UCC model to observe the flow inside the UCC. In this study, an ethylene igniter torch was characterized for the UCC and identified improved vortex trapping at higher flow rates relative to the cavity flow. This result is indicative of a more consistent temperature distribution entering the turbine. These results differ from those of previous experiments, but give a good basis for studying the effects of g-loading on the flow.[6]

2.6 Laser Diagnostics Techniques

Laser diagnostic techniques have emerged as an extremely powerful tool for combustion analysis. They provide non-invasive, real time data gathering capabilities never before possible. Traditional measuring devices, such as thermocouples and probes, cannot typically withstand the high temperatures of a combusting environment. Furthermore, they have to be physically inserted into the flow causing a disruption ultimately changing the flow dynamics. Laser diagnostics avoid these problems and can also interrogate areas within a flow never before physically accessible. This gives invaluable insight to combustion flow dynamics and characteristics, which enables extensive research and design to further promote combustion capabilities.

There are various techniques available to perform laser spectroscopy on a medium of interest. The AFIT COAL laboratory currently possesses the capability to perform Planar Laser Induced Fluorescence (PLIF), Particle Image Velocimetry (PIV), and Tunable-Diode Laser-Based Absorption Spectroscopy (TDLAS) to name a few. Of these options, this research will focus on utilizing TDLAS.

2.6.1 Tunable Diode Laser-Based Absorption Spectroscopy

Tunable Diode Laser Absorption Spectroscopy (TDLAS) is a laser diagnostic technique employing a coherent Ultra-Violet (UV) beam of light through a medium of interest.

TDLAS exploits the molecular absorption of energy. Molecular absorption occurs when the energy is taken up by a molecule and excites an energy state of a molecule to a higher energy level. The specific energy states targeted by this research are the molecule's vibration and rotation modes. Movement between these energy states is the electronic transition of the molecule, as seen in Figure 12.[30]

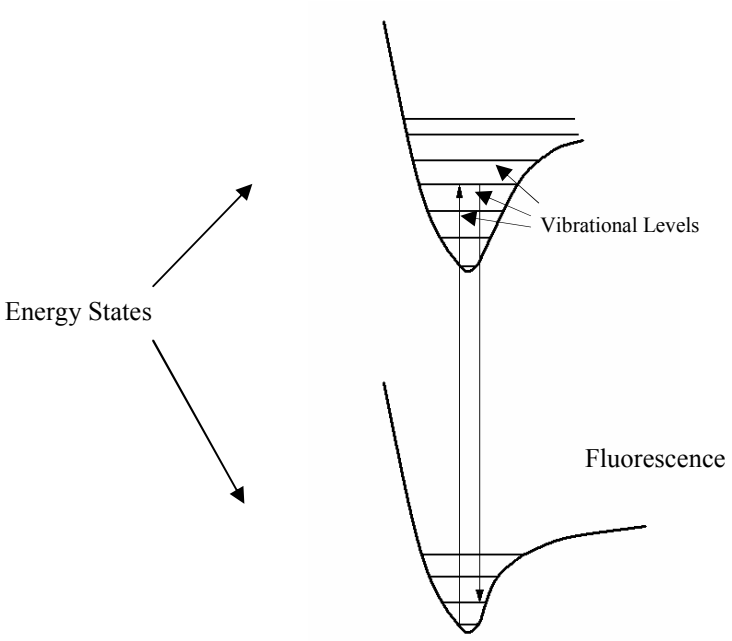

Figure 12: The X and A energy states with sub vibrational levels shown

The ground state for electrons of a given molecule are shown as the X energy

state. The upward pointing arrow indicates the excitation movement of a molecule from energy state X to higher energy state A. The horizontal lines represent the vibrational levels within each energy state. Shown in Figure 13, there exist many variations of rotational energy states within each vibrational level.

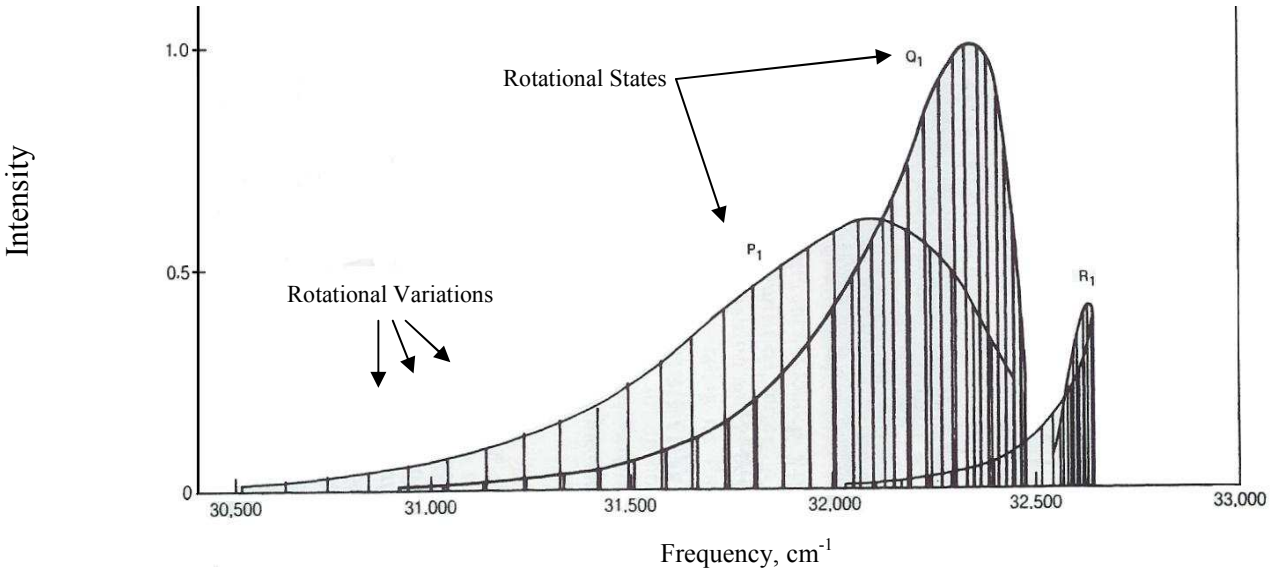

Figure 13: Illustration of the rotational structure of a vibrational level (Adapted from Eckbreth, 1998).

These rotational states are identifies through a letter-number combination followed by the specific variation in parenthesis, i.e. $P_2(10)$. These states are excited by specific wavelengths of light, and are generally referred to as "lines". Each molecule or species of interest have many unique absorption lines with a specific range of frequencies.[30]

In the TDLAS approach, the laser is tuned to a characteristic absorption line in the

spectrum of a desired species of interest. As the laser passes through a medium, a reduction in the signal intensity of the laser is measured by a photodiode. The difference in signal intensity is then used to determine temperatures as well as species concentrations through Beer's Law, as previously discussed. The shape of the resulting absorption spectra is curve fit using a Maxwell-Boltzmann expression.

2.6.2 Doppler Broadening

Doppler Broadening is the broadening of spectral lines as a result of the Doppler Effect. The Doppler Effect occurs when molecules become excited, due to a temperature increase, and shift the frequency of the line (emitted photons). The varying velocities of the molecules in the gas create several small shifts which, when combined, broaden the line. The resulting line shape is called the Doppler profile. The derivation of the Maxwell-Boltzmann distribution is an expression for the Doppler profile and is seen in equation 10.

$$g_D(\nu) = \frac{c}{\nu_0}\sqrt{\frac{m}{2\pi kT}}\ exp\left[-4\ln 2\frac{(\nu-\nu_0)^2}{\Delta\nu_D{}^2}\right] \tag{10}$$

where $g_D(\nu)$ is the line shape function, c is the speed of light, ν_0 is the transition center frequency, m is the molecular mass, k is Boltzmann's constant, T is temperature, and $\Delta\nu_D$ is the transition width. The Doppler line is mathematically prescribed as a Gaussian function and the line shape function, $g_D(\nu)$, is defined such that the integral is equal to 1.[30]

Of significance to the TDLAS method as well, $\Delta\nu_D$ is the transition full width at

half maximum (FWHM) height and is expressed as

$$\Delta\nu_D = \frac{2\nu_0}{c}\sqrt{\frac{2\ln 2\ kT}{m}} \tag{11}$$

For a given species, i.e., a specific m , the Doppler width, $\Delta\nu_D$, is primarily a function of temperature. This indicates the line width can determine temperature, provided line broadening is mostly a result of the Doppler Effect. This is typically the case at low pressures.[30] However, it is important to note pressure, or collisional, broadening needs to be considered as it does pose the possibility of an effect on experimental data when comparing results with theoretical calculations from programs such as LIFBASE and CEA.

2.6.3 Pressure Broadening

Fourier analysis states an infinitely long sinusoidal wave train is monochromatic. For a wave train of finite time (τ), a spread in frequency will be present. This is represented as

$$\Delta\nu_c = \frac{1}{\pi\tau} \tag{12}$$

A molecule interacting with radiation, (i.e. absorbing the laser light) is likely to collide with other molecules. When these collisions occur, they cause line broadening and shifting of the spectral line, known as collisional broadening (pressure broadening) and collisional shift. The statistically averaged effect of the collisions determines the line shape and is represented by the function

$$g_c(\nu) = \frac{\Delta\nu_c}{2\pi} \frac{1}{(\nu - \nu_o)^2 + \left[\frac{(\Delta\nu)_c}{2}\right]^2} \tag{13}$$

This is also referred to as the "Lorentzian" line shape as it was first performed by H.A. Lorentz. Just as the Doppler line shape function is defined such that the overall integral is equal to unity, so too the Lorentzian line shape function. For room temperature at 1 atm, pressure broadening usually dominates Doppler broadening by an order of magnitude. However, when the temperature is increased to around 2000 K, pressure and Doppler broadening lines are comparable to one another.[30]

2.6.4 Voigt Profile

When neither Doppler broadening nor pressure broadening dominates, they are both combined. The resultant conjugate line shape is called a Voigt profile. The Voigt line profile is mathematically represented as

$$g(\nu) = 2\sqrt{\frac{\ln 2}{\pi}} \frac{V(a,x)}{\Delta\nu_D} \tag{14}$$

Where $V(a,x)$ is the Voigt profile, and a and x are defined as

$$a = \sqrt{\ln 2} \frac{\Delta\nu_c}{\Delta\nu_D} \tag{15}$$

$$x = 2\sqrt{\ln 2} \frac{(\nu - \nu_o)}{\Delta\nu_D} \tag{16}$$

The Voigt profile essentially sums the pressure broadening profile, centered about a line frequency, weighted by the Doppler profile at the same frequency. The Voigt profile becomes Gaussian shaped when the parameter a is bound by $0 < a < 1$. This

indicates the dominance of Doppler broadening. However, as a increases proportionally to pressure increase, the Voigt profile develops broad wings. This continues up to the point to where a = 2, where pressure broadening dominates and the line profile is predominantly Lorentzian.[30]

2.7 Laser Structure

Generation of the wavelength necessary to detect the OH radical in combustion products is accomplished through a laser mixing technique. In doing so, flame location, temperature profiles, and concentration profiles are able to be ascertained through resultant data. The TDLAS system utilized in this research is based on the generation of UV radiation at 313.5 nm by sum-frequency mixing of the output of a 763 nm distributed-feedback (DFB) diode laser with that of a 532 nm diode-pumped, frequency-doubled neodymium-doped yttrium orthovanadate (Nd:YVO_4) laser in a β-barium borate (β-BBO) crystal.[25]

2.7.1 Nd:YVO_4 Lasers

If a laser survey is conducted, one would find a myriad of lasers available for just as many uses. Concentrating on combustion diagnostics, this list can be narrowed. One such laser that is commonly found is the neodymium-doped yttrium orthovanadate, Nd:YVO_4, laser. The Nd:YVO_4 laser is pumped by flash lamps or laser diodes and can operate in pulsed or continuous mode. The laser configuration for the AFIT COAL lab is the laser diode pumped, pulsed, frequency doubled Nd: YVO_4.

Laser diode pumping provides excitation energy necessary for lasing to occur in

trivalent neodymium ions (Nd^{3+}), housed in a yttrium orthovanadate (Y_3VO_4) crystalline host material, also called the gain medium.[30] Laser pumping is the act of transferring energy from an external source into the gain medium of the laser. Energy absorption by the medium ions results in excited states in its atoms. As the number of particles in one excited state exceeds the number of particles in the ground state, population inversion occurs. Population inversion is where more atoms exist in an excited state than in a lower energy state. Once this is achieved, the medium can act as a laser.

2.7.2 Distributed-Feedback Diode Lasers

Distributed-Feedback Diode Lasers (DFB) are a type of laser that has diffraction grating as the structure for the active region of the device. Diffraction grating is an optical component with a regular pattern. This pattern diffracts light into multiple beams all traveling in different directions. The grating provides optical feedback for the laser, thereby eliminating the need for mirrors in the optical cavity. The grating is configured to only reflect a narrow band of wavelengths, which produces a narrow line width of laser output.

By altering the temperature of the device, the pitch of the grating can be varied due to thermal expansion. This makes the reflection wavelength, and thus the laser output wavelength, variable, thereby producing a tunable laser. Altering the power current to the device will also tune the output laser. This is of significant importance, as it allows for analysis over a broader range of wavelengths.[31]

3 Methodology

3.1 Objective Achievement Methods

In order to satisfy the objectives, the following steps were taken:

1. *Construction of the TDLAS System*. Prior to any experimental procedures, the TDLAS system must first be constructed. A configuration similar to those in Meyer et al. and Anderson et al. will be utilized for the COAL laboratory.
2. *Calibration and Validation of the TDLAS System*. Following construction of the TDLAS system, the lasers must be aligned properly, calibrated, and verified. Validation of the system will be accomplished by comparing known theoretical data to that collected with the system for a laminar hydrogen-air flame produced by a Hencken burner.
3. *Characterization of the TDLAS for Turbulent Environments*. Prior to the TDLAS systems utilization for experimental data in the UCC, it must first be characterized in a turbulent regime. For this, a jet diffusion flame will be employed. Known data for temperatures as well as flame behavior will be utilized to verify operation, as well as characterize the system for a turbulent environment.
4. *Update Operational Procedures*. AFIT's COAL laboratory is an ever expanding, evolving project. It is designed and re-designed to employ

the latest, stat-of-the art laser diagnostics on cutting edge research topics. It is imperative that each researcher write operational procedures for new systems and update existing procedures when necessary. With this in mind, procedures for operating the TDLAS system will be written, procedures for operation of the jet for the diffusion flame will be written, and operation of the Hencken burner as well as the UCC will be reviewed.

5. *Performance Calculations*. Several parameters from the Hencken flame and turbulent jet flame will be gathered using Lab-View software. These parameters will then be used to calculate temperature and OH concentration profiles for the flames.

3.2 TDLAS Assembly

In order to perform absorption spectroscopy analysis for various combustion environments, the system must be built. Since there are no commercially available sensors for high speed detection of the OH radical, one must be constructed. This was previously accomplished by Meyers et al. The same general configuration was followed for the system in the COAL laboratory.[27]

The TDLAS system was constructed entirely on one end of an optics table in the AFIT COAL laboratory. The two lasers utilized were a Coherent Verdi-5 Nd:YVO_4 unit and the Cheetah DFB diode unit. The optical set up and system assembly was completed by myself and Stanislav Kostka, a contracted exchange PhD student from the University

of Connecticut. The Nd:YVO_4 laser produces a pulsed 532 nm beam and the DFB laser produces a 763 nm beam. The beams are focused and mixed in a BBO crystal for a sum-frequency generated UV beam at 313.5 nm. The configuration of some of the optical components can be seen in Figure 14.

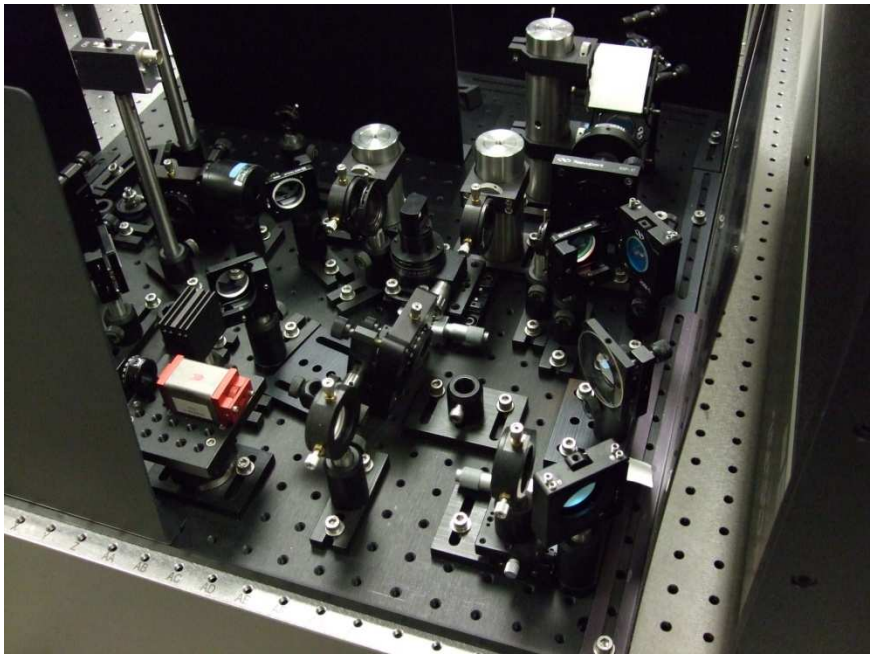

Figure 14: Optics set up for TDLAS system

As the beam passes through the optics, power output and wavelength can be measured without disrupting the path. This can be viewed in the experimental layout shown in Figure 15.

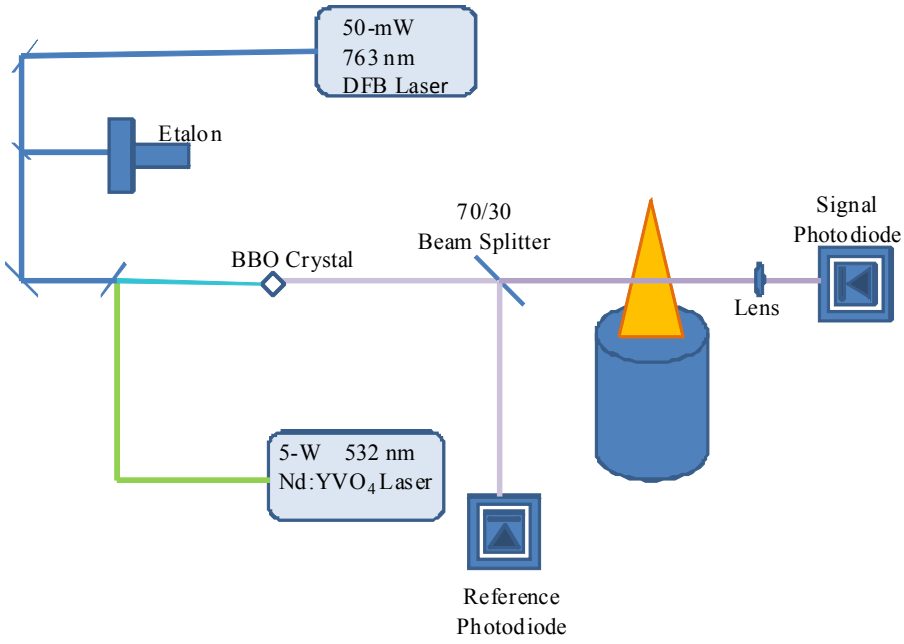

Figure 15: Experimental Layout

Once the set up was complete, the laser beam needed to be focused and aligned. This was accomplished by adjusting the lenses and other optical equipment on the table. A properly focused and aligned beam appears as a bright circular dot of light against a white card, not fuzzy or smeared in nature, nor a line, bar, or oval shape. One of the steps in the alignment process can be viewed in Figure 16. Note the card used for assessment of the laser focusing is indicated by the red arrow.

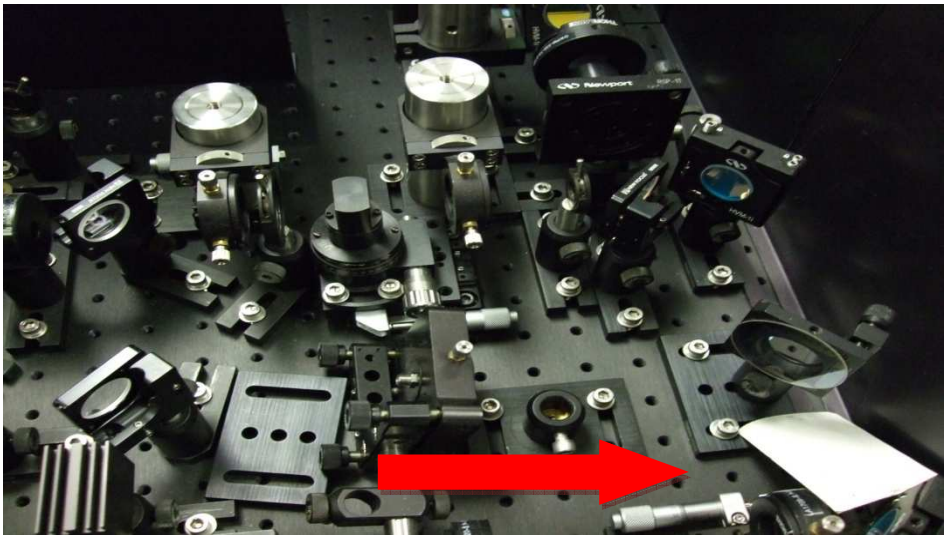

Figure 16: Alignment process for the lasers

The alignment process is especially important for the TDLAS system as two lasers are sum-frequency combined. As a result, the Nd:YVO_4 and DFB laser alignment must be very precise and the beams must align with each other perfectly, prior to mixing in the BBO crystal, to produce the necessary 313.5 nm frequency needed for the research.

Once the beam is aligned and focused through the entire system and into the photodiode, which will collect the information once the beam has passed through the flame, data collection can take place. Operational and safety procedures for the lasers are included in the laboratory procedures.

3.2.1 Additional System Components

An important component of the system is the Stanford Research Systems SR560 low noise preamplifier, show in Figure 17. For the TDLAS system, there were two of

these components, one for the reference signal, and one for the data signal.

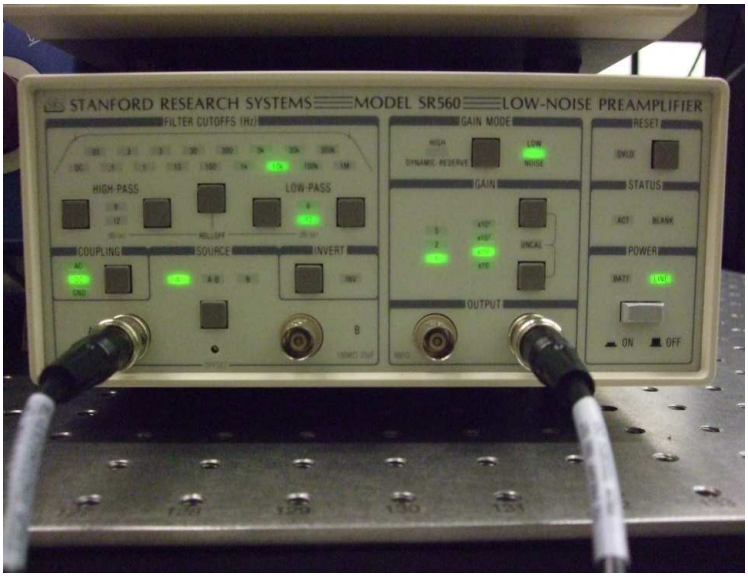

Figure 17: SR560 preamplifier

This piece of equipment performs band pass filtering at 10 kHz. The resulting signal leaves the low impedance (50Ω) output of the preamplifier.

A component used to measure power output in the form of voltages is an oscilloscope. This particular piece of equipment allows for the measurement of signal voltages and provides a visual output on a screen. This component can be seen in Figure 18.

Figure 18: Oscilloscope used for signal tracking

The oscilloscope was used because it not only permits visual verification of laser power, and thus operation, but it also provides observation of the exact shape of the waveform. This is important for absorption spectroscopy as a small divot, or indentation in the up ramp and down ramp of a signal indicates absorption is occurring, the system is operational, and the data being collected should be useful.

The Pilot laser diode controller for the Cheetah DFB laser is an integral piece of equipment. Commonly mistaken as a power supply, this component provides constant current to the DFB laser.

Figure 19: DFB laser diode controller

Though it may seem like semantics when referring to a constant current input and a power supply, they are quite different. A power supply can be defined as a general purpose device that provides bulk power to an electrical circuit, whereas a laser diode controller is a specialized device used specifically to provide current to a laser diode. A typical power supply provides a regulated source of direct current (DC) power and is regulated by two knobs: one that sets a voltage limit and one that sets a current limit. Once the power supply is initiated, electrical output increases until one of the two limits is reached, where output is then maintained.[32]

A sharp initial rise in voltage as current is applied is a characteristic behavior of laser diodes. Upon surpassing the current threshold, voltage rise is very gradual with further increase in current. For this very reason, utilizing a power supply to drive a laser diode is pernicious. When initially turning on a power supply, the voltage servo detects voltage output below target and increases the output rapidly. While this is occurring, the current is well below its set limit and therefore the power supply's current limiter is not

active. Once the output voltage limit to the laser diode is met, the current rises abruptly, triggering the current limiter. The current limiter cannot act instantaneously to stop further increase in current, and thus an excessive current is momentarily delivered to the laser diode. Repeated exposure to excess current will drastically shorten the lifespan of a laser diode.[32]

The laser diode controller is designed as a constant current source and does not even have a constant voltage mode of operation. There is one knob and one servo loop, which allows the design to all but eliminate the possibility of current overshoot. While the primary purpose of the controller is to provide current, if any anomaly is detected, the controller immediately terminates output, thus protecting the laser diode from damage and premature component failure.[32]

3.3 Combustion System Calibration and Operation

To adequately conduct research in the AFIT COAL laboratory, it was necessary for some initial calibration and calculation of several components and parameters. This was necessary as to operate the several test devices safely and effectively.

3.3.1 Theoretical Calculations

In order to effectively operate the combustion test devices, acquire effective data, and accurately interpret results, theory must be correctly applied to the process. For this experiment, this requires that combustion parameters must be theoretically calculated assuming complete, equilibrium combustion has occurred. The

basis for this theory has been previously discussed, but will be demonstrated forthwith.

Calculation of varying equivalence ratios (Φ) for the testing environment was accomplished for hydrogen-air flame for Hencken burner operation. For complete combustion of Hencken flame, the chemical equation is:

$$2H_2+(O_2+3.76N_2)\rightarrow 2H_2O+3.76N_2 \tag{17}$$

Utilizing equation (5), the fuel-to-air ration at stoichiometric conditions (Φ=1) can be found by

$$\left(A/F\right)_{STO}=\frac{4.76}{2}=2.38 \tag{18}$$

Holding air at a constant flow rate of 30 SLPM, varying ϕ will also vary fuel flow rate by implementing equation (6) as illustrated below:

$$\phi=\frac{2.38\ F}{30} \tag{19}$$

Utilizing this method, several Hydrogen flow rates were calculated and were applied for operation of the Hencken burner. The tabulated values appear below in Table 2.

Table 2: H2-air flame ϕ and fuel flow rates for constant air at 30SLPM

Φ	Fuel (SLPM)
0.4	14.0
0.5	17.5
0.6	21.0
0.7	24.5
0.8	28.0
0.9	31.5
1.0	35.0
1.1	38.5
1.2	42.0
1.3	45.5
1.4	49.0

Calculations for the turbulent jet flame using Ethylene (C_2H_4) as the fuel were based on Reynolds number (Re) rather than equivalence ratio, as this is flow emanating from a pipe. By varying Re, the percentage of C_2H_4 needed could be calculated. Observing the equation for Re:

$$Re = \frac{\rho V D}{\mu} \tag{20}$$

where ρ is the density of the fuel, V is the velocity, D is the jet diameter, and μ is the dynamic viscosity of the fuel. Designating Re and knowing all parameters other parameters, velocity can be calculated and utilized to find fuel flow percentage for the jet diffusion flame. Calculation of velocity for a corresponding Re number is shown by rearranging equation (20) as:

$$V = \frac{Re\,\mu}{\rho\, D} \tag{21}$$

Once velocity is known, volumetric flow rate ($\dot{V}$) can be calculated by:

$$\dot{V} = V * A \tag{22}$$

where A is the area of the jet tube. $\dot{V}$ is in units of m^3/s and needs to be converted to SLPM. This is accomplished by multiplying $\dot{V}$ by 60,000. The resultant fuel flow rates corresponding to the Re are show in Table 3.

Table 3: Fuel flow rates at corresponding Re for the turbulent jet

Re	**% C_2H_4**
500	1.09
1000	2.18
1500	3.27
2000	4.37
2500	5.46
3000	6.55
3500	7.64
3750	8.19
4000	8.73
4250	9.28
4500	9.82
4750	10.37
5000	10.91
5250	11.46
5500	12.00
5750	12.55

3.3.2 Mass Flow Controller Calibration

The ability to control the flow rates of any substance utilized for the COAL laboratory combustion system is critical in order to produce accurate data. Anderson's thesis addresses the theory behind the control methods.[33] All gases delivered to any combustion device are controlled by MKS ALTA digital mass flow controllers, shown in Figure 20.

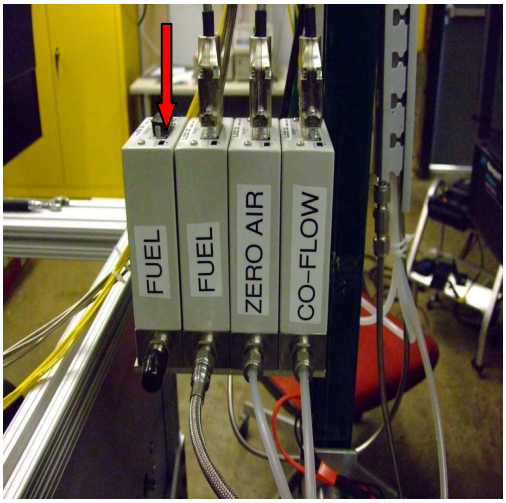

Figure 20: MKS ALTA digital mass flow controllers. Red arrow points to the zero reset button[5]

Though they appear identical, each mass flow controller is different for this lab setup. Each controller is set for a specific maximum flow rate. The maximum flow rate values for these controllers is 5, 10, 30 and 50 SLPM. Any controller can be used for any gas, and therefore require frequent recalibration.

For proper calibration, the MKS ALTA mass flow controllers have to be zeroed out. It is important that the system be turned on and permitted to warm up for a

minimum of thirty minutes. Once the warm up period is passed, calibration can be initiated. First, a no-flow condition through the controllers must exist. Once this is achieved, the zero reset button on top of each controller can be pressed, resetting the mechanism inside the controller to the no-flow position.[5]

An MKS 247 four channel power supply / readout, shown in Figure 21, operates the mass flow controllers. This piece of equipment permits adjustments of the flow setting for the controllers by the operator of the system. These adjustments can be made in either SLPM or percentages of total flow capacity of the controller. Hankins found that the using percentages of flow capacity provides the easiest and most accurate method with calibration curves.[5]

Figure 21: MKS 247 four channel readout [5]

Each channel corresponds to a mass flow controller. The display on the MKS 247 should read all zeros when the corresponding mass flow controller has been zeroed out. Should this not occur, adjustments can be made by using a jewelers screwdriver to turn the small tuning screw located under Z on the front panel for the respective channel until

the display reads all zeros. Of notable interest that has been documented in both reference 5 and 6, as well as this research, is when positive pressure is applied to the controllers, there is a small amount of flow permitted through. The controllers read the flow and the output is displayed on the readout panel. Rater were reported as high as 0.9%, but percentages of only between 0.2%-0.4% were observed for this study.[5,6]

The next calibration to be made is for flow through the controllers. For this calibration, the BIOS Definer 220-H was employed to give a precise measurement of the flow rates through the controllers. Shown in Figure 22, this stand-alone unit is affixed in-line and downstream of the controller.

Figure 22: BIOS International Corporation Definer 220-H flow meter calibration device[5]

The ALTA mass flow controllers are pre calibrated by the factory for a specific gas. If a controller is mated with the gas it was precalibrated for, flow rates at various settings can be predicted with a factory provided table of gas correction factors. These

numbers are utilized for recalibration and tuning of the MKS 2747 readout display. It is recommended that a range of flow settings be tested to ensure the valve responds linearly to inputs. In order to test a flow setting, the "Set Point" toggle switch should be held in the up position while simultaneously setting the desired flow rate by adjusting the tuning screw immediately to the right of the switch. Upon setting the flow rate, the toggle switch can be released and placed in the "Read" position. The selected channel's operating switch must be placed in the "On" position. At this juncture, the BIOS flow meter will take ten measurements and provide a digital readout for the average of the measurements. The meter will continue this loop unless otherwise physically paused or turned off. The anticipated flow rate that has been previously calculated and the average value should match. If they do not, then adjustment of the tuning knob is required until the averaged measure flow rate and the set flow rate coincide. Repeating this process for several settings is required for complete calibration. Upon completion of these calibrations, the mass flow controllers are prepared for use.

As insinuated, these mass flow controllers are not always paired with the gas the factory precalibrated them for. If this is the case, the controller must be characterized to the gas to be used. This is done by taking measurements for a full range of flow settings of the controller and then determining the average flow rate per setting. These parameters can be used to create plots, such as Figure 23.

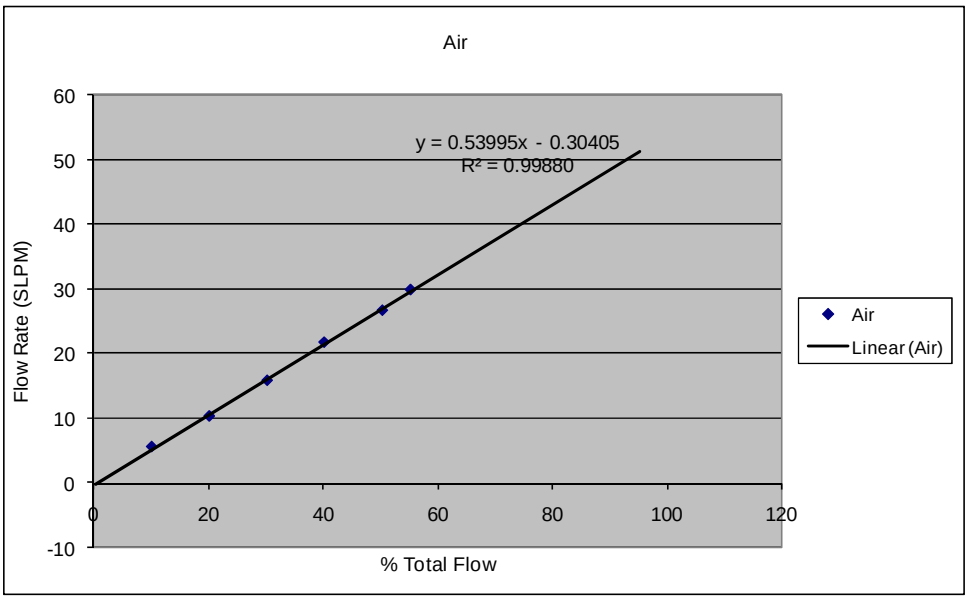

Figure 23: Mass flow meter calibration plot (Air)

Once the data is plotted, a linear trend line is fitted to the data and provides an equation to define the relationship. This equation is then used as the formula for calculating the necessary settings on the MKS 247 readout to get the desired flow rates. Controllers were calibrated to Air, Hydrogen, Nitrogen, and Ethylene using the above described process. The H_2, N_2, and C_2H_4 curve fits are shown in Figure 24.

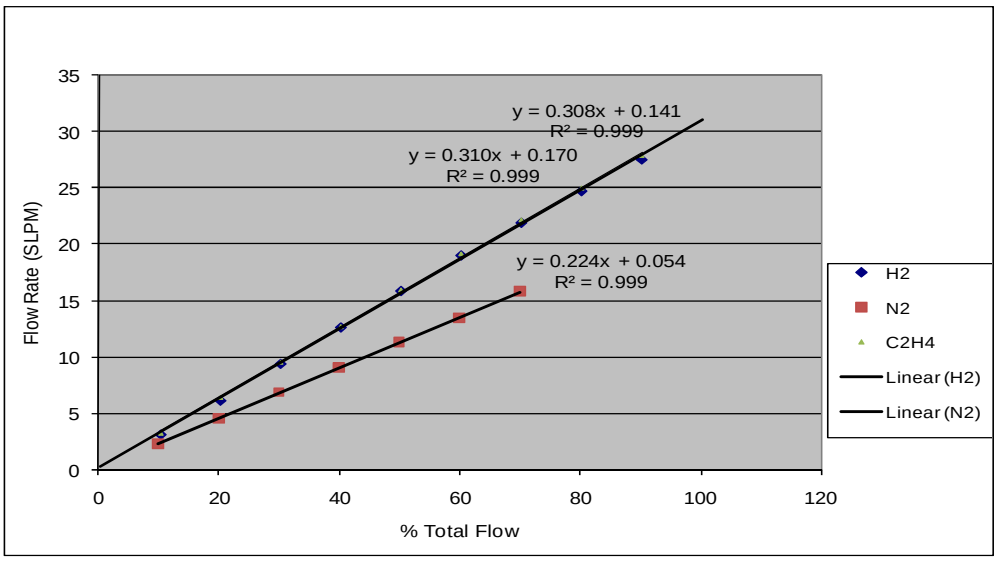

Figure 24: Mass flow meter calibration plot for H_2, N_2, C_2H_4

3.3.3 Hencken Burner Operation

The Hencken burner is relatively simple to operate. It produces a premixed, laminar flame that has been well characterized by many research efforts. For this very reason, the Hencken flame was chosen for calibration of the TDLAS system. Operating procedure for the Hencken burner will now be discussed.

It is first necessary to turn on the MKS 247control panel. As previously mentioned, this piece of equipment has a 30 minute warm up time. Once the control panel is on, the laser should also be turned on in order to permit a minimum of 20 minutes of warm up time as well. During the equipment warm up period, the tanks in the tank farm should be opened. The tank farm is located outside on the back side of the building, just outside and west of the exit door for lab room 258. For Hencken burner

operation, the hydrogen, air and nitrogen tanks need to be opened. Nitrogen is needed as the burner provides for a co-flow of an inert gas. This co-flow is necessary to keep the flame laminar far from the surface of the burner as well as prevent mixing with ambient air. Should nitrogen be unavailable, another inert gas may be used. The use of co-flow is further discussed in Koether's thesis.[34]

After the tanks are opened, the valves located along the east wall of the COAL laboratory must also be opened to permit flow of the gasses into the system and charge the lines up to the mass flow controllers. This positive pressure on the inlet of the mass flow controllers is essential in order to prevent damages or malfunction.[5] Once the warm up has occurred, the mass flow controllers can be set to the desired flow percentages that correspond to the operating equivalence ratio. Keother's thesis provides a detailed description of this procedure. The Hencken burner can now be lit in accordance with the procedures described in Hankin's thesis.

The actual burner employed for this research has a square array of small diameter fuel and oxidizer tubes. It carries an outer dimension of 38 x 38 mm and an inner burning surface dimension of 24.5 x 24.5 mm. The burner can be seen in Figure 25.

Figure 25: Hencken burned utilized for calibration of the TDLAS system in the AFIT COAL Laboratory

The research performed by Meyer et al. was referenced to provide operating parameters and laser placement. For calibration and validation purposes, it was noted that the measurements within the range from 5-10 mm above the surface of the burner gave the most agreement with both adiabatic and corrected numerical predictions.[25] While the air flow rate was held constant, the fuel(H_2) flow rate was changed in correlation to the appropriate Φ. The co-flow rate is also set and is not varied as its function is to preserve the laminar nature of the flame for analytical purposes, and does not contribute in the actual combustion process.

Shut down procedures for the Hencken burner are located in reference 5. It is important to note here that the valves controlled by Lab-View should be the last part of

the combustion system equipment closed and are never to be closed while the mass flow controllers are still on. Closure of these valves will cause the mass flow controllers to spike open and possibly become lodged in the open position. Should it become necessary, detailed procedures for safely bleeding the gas lines is provided in Hankins thesis.[5]

3.3.4 Turbulent Jet Operation

Just like the Hencken burner, the turbulent jet is a simple system, only it generates a turbulent jet diffusion flame. This turbulent flame is used for characterization of the TDLAS system for a turbulent regime.

Start up procedure for the turbulent jet is very similar to that for the Hencken burner. The mass flow controller system and laser system must be warmed up, appropriate tanks in the tank farm must be opened, and the correlating valves on the lab wall must be opened. The lighting and shutdown procedures are the same for the Hencken burner, which are found in reference 5. The turbulent jet is operated with an ethylene-nitrogen mixture, therefore the ethylene and nitrogen lines should be opened. Ethylene was chosen as it most closely represents a typical hydrocarbon fuel in a combustion device, and therefore gives a better characterization of expected ranges for temperatures and OH concentrations. Figure 26 shows the turbulent jet flame.

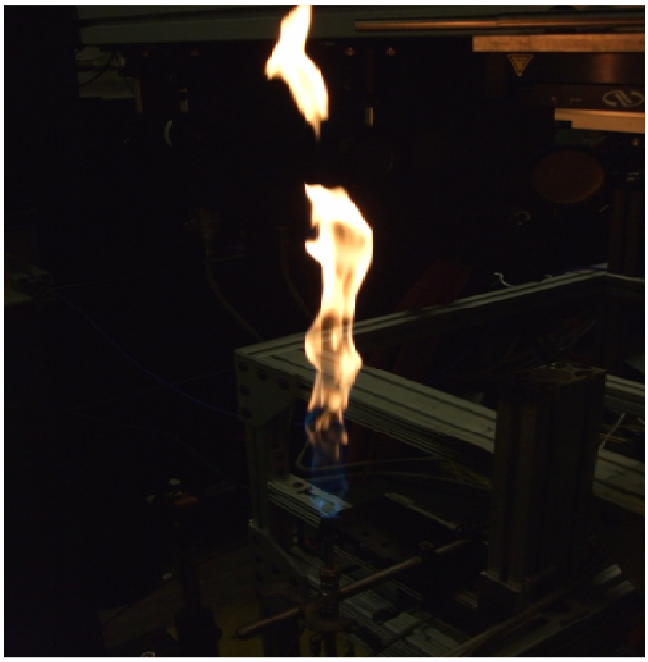

Figure 26: Turbulent jet diffusion flame

The jet diffusion flame characterization of the laser system was accomplished by pitching the laser beam through the turbulent flame and collecting the data through a photodiode on the other side. The vertical position of the laser was twenty diameters above the outlet of the jet and was centered horizontally. Data was gathered for a range of flow rates governed by varying Reynolds numbers, beginning in the laminar Re range and terminating well in the turbulent Re range. At the highest Re, the laser beam was traversed horizontally across the half width of the flame. This was done to analyze the performance of the TDLAS system for reading the profile of a turbulent flame.

3.4 Data Collection and Analysis

The COAL laboratory is outfitted with state-of-the art equipment and technology, which allows for more efficient data collection and recording. The lab set up currently consists of three control stations for operation of the various laser diagnostic systems. The computer control station permits operation of all systems to be controlled from one central location, and can be seen in Figure 27.

Figure 27: Computer Control Station[5]

The design and set up of the computer control station was accomplished by Anderson and details are found in his thesis.[33] The other two stations are the laser control station and the camera control station. No high-speed video was taken and the camera system was not utilized for this research, however, it is part of the lab set-up and is worthy of recognition. The laser control station design and capabilities are detailed in reference 34. Both systems can be observed in Figure 28 and Figure 29.

Figure 28: Laser Control Station

Figure 29: Camera control station

Various software and freeware packages are used in data collection and analysis. Lab-View is software utilized for operational control of most of the lab as well as for data gathering, reduction, and analysis for the TDLAS system. CEA (Chemical Equilibrium with Applications) is freeware created by NASA. This computer program calculates product concentrations for any set of reactants assuming chemical equilibrium.[35]

LIFBASE is also a free application. It is a spectral simulation database, which holds electronic transition data for diatomic molecules and can provide absorption or emission simulation.[36] MATLAB is a programming language used for complex calculations not otherwise easily performed.

3.4.1 Lab-View

Lab-View is a program from National Instruments that provides the foundation for system control and data acquisition for the COAL laboratory. The Virtual Instrument (VI) interface controls all fuel and air flowing to the testing rig. Furthermore, it provides for adjustments of the state of the flows, and is the core for most data acquisitions of experiments performed in the laboratory. A view of the VI designed by Anderson is seen in Figure 30.

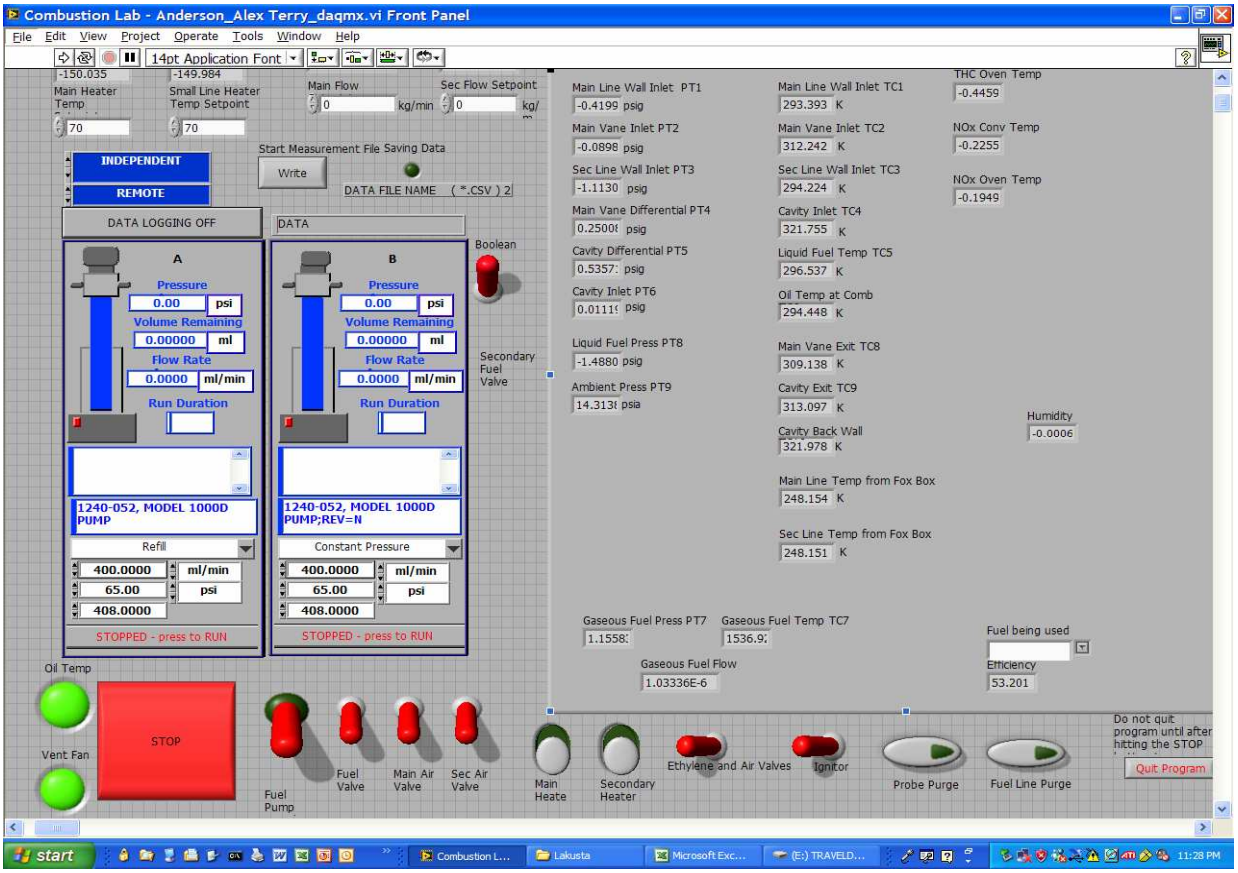

Figure 30: Lab-View VI control interface for the combustion system[6]

This was for control of the combustion system. Lab-View was also installed on the TDLAS computer control system that resides on the laser control station. The programming and control of the Lab-View software utilized on this computer operated the laser system as well as collected the data. An analysis program was also written for interpretation of the collected data. Stanislav Kostka, an exchange PhD student from the University of Connecticut, designed and implemented the Lab-View programs used for the TDLAS control interface. A screen shot of the VI interface for the laser system is

shown in Figure 31.

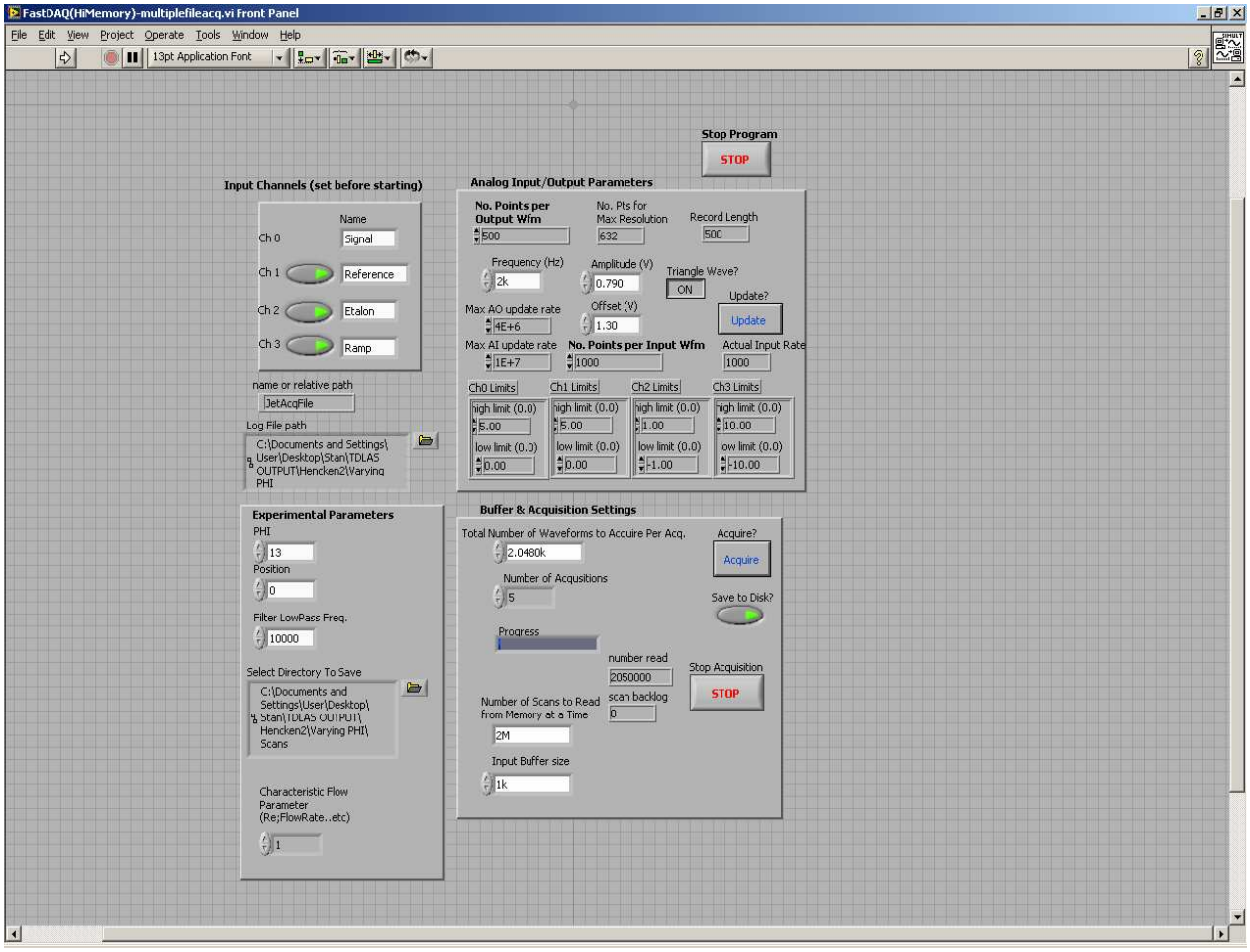

Figure 31: Lab-View VI interface control of TDLAS laser system

3.4.2 CEA

CEA was used to provide some of the theoretical calculations to verify experimental data against. CEA is a free software developed by researchers at NASA Glenn reserch center for equilibrium claculation of chemical reactions. CEA was born out of the need for a database of thermodynamic data to be utilized in the calculation of chemical equilibrium composition and rocket performance. CEA calculations are for the

chemical equilibrium product concentrations from any set of given reactants. CEA determines the thermodynamic and transport properties of the product mixture, assuming equilibrium.[35] Though experimental reaction products are never at equilibrium, comparison to equilibrium data provides a solid basis for analysis.

3.4.3 LIFBASE

LIFBASE is a free system that simulates the electronic transition behavior for a diatomic molecule. This can be performed for either absorption or emission, and includes options for consideration of Doppler and pressure broadening. LIFBASE was used to calculate and compare theoretical line broadening for OH of absorption. A screenshot of the program can be seen in Figure 32.

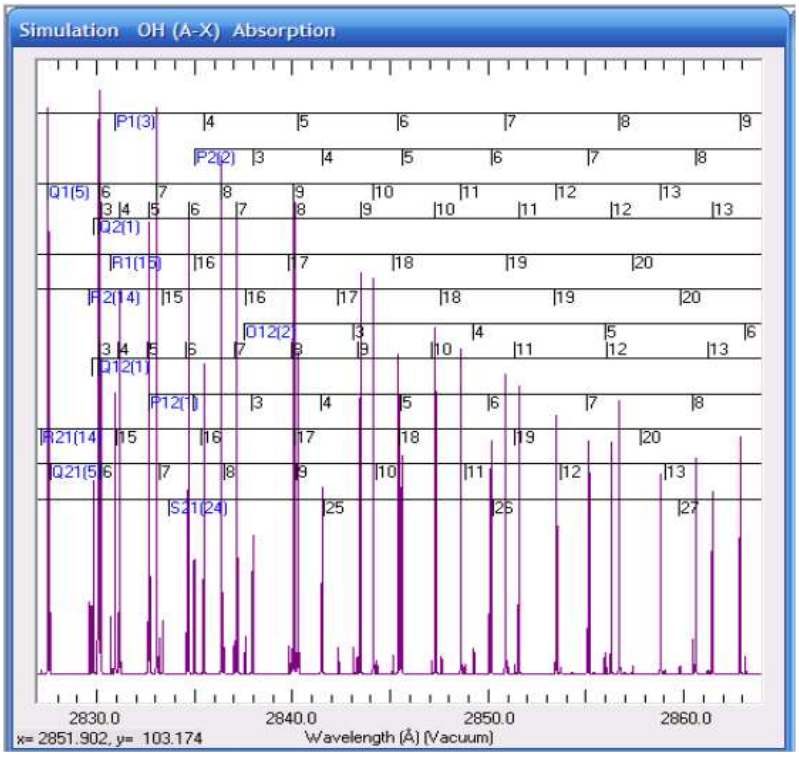

Figure 32: LIFBASE program providing theoretical calculations for data

analysis. Wavelengths are given in Angstroms[5]

The vertical peaks indicate wavelengths at which OH absorbs incident light, i.e., laser light. The height is the relative OH absorption at the given wavelength. Normalization is done by signal strength where the highest line is normalized to 100.[5] LIFBASE simulation calcualtions are performed for a range of temperature, which give varying OH concentraion. As OH concentration varies, so does signal strength at each temperature. This is used for experimental data correlation to ensure accuracy.[5]

3.4.4 MATLAB

MATLAB is a powerful computational language designed to perform fast calculations. It was used for calculating data from this experiment that would otherwise require an inordinate amount of time to assess. Code for temperature and OH concentrations was written and executed for both the laminar Hencken flame as well as the turbulent jet diffusion flame. The code was an alpha-numeric compilation of constants and equations used for the proper computation and calculation of temperatures and OH concentrations for the above mentioned flames. A copy of this code is attached in Appendix A.

Turbulent Fluctuations

The random nature of turbulence does not lend itself to direct calculations of characteristics, which suggests that statistical methods will provide insight. Given any quantity U, the average value of any power (ν),

$$\overline{U^{\nu}} = \int_{-\infty}^{+\infty} U^{\nu} P(U) dU \tag{23}$$

where P(U) is the probability density function. This is called the moment of order ν, or the ν^{th} moment of U. The mean of U is the moment of order 1, or the 1st moment of U. [38]

The central moments give various characteristics of random data and are defined by

$$\mu_{\nu} = \overline{\left(U - \overline{U}\right)^{\nu}} \tag{24}$$

For integer $\nu > 1$, the central moments are used to understand different aspects of variable data, i.e. turbulent fluctuations. [38]

As previously mentioned, $\overline{U}$ is the average of any value U over a period of time. The fluctuation of U is defined as

$$u_i = U_i - \overline{U}_i \tag{25}$$

Equation 25 is typically representative of turbulence. Turbulent intensity can be measued in different i directions using the standard deviation. Standard deviation can be shown as

$$\sigma = u_i' = \left(\overline{u_i^2}\right)^{1/2} \tag{26}$$

Turbulent intensity (TI) is a scale characterizing the magnitude of turbulent fluctuations expressed as a percent and is defined as

$$TI = \frac{u'}{U} \tag{27}$$

TI is used to understand to how turbulent the quantity of interest is. Low turbulence, or near laminar, cases typically have a TI of approximately 1% or less. Moderately turbulent cases are considered as having between 1-5 % TI, and instance of >5% TI are highly turbulent. [38]

4 Results and Analysis

4.1 TDLAS Results for the Hencken Burner

Validation of the TDLAS system was validated in the COAL lab by taking data of a well characterized laminar hydrogen-air flame produced by a Hencken burner. Temperatures and OH concentration were determined for various equivalence ratios. Temperature and concentration can be determined by measuring the difference between the reference signal and the data signal, as previously discussed. This signal broadening then provides direct correlation to the temperature and OH concentration in the flame. Theoretical data from CEA and LIFBASE for these same experimental conditions was gathered and compared to the experimental results for accuracy. Several sets of data were gathered for each condition and are discussed forthwith.

4.1.1 Theoretical Data and Calculations

CEA was used to obtain flame temperature and OH concentration as they relate to equivalence ratio (Φ). As discussed in reference 5, there was no appreciable difference in altering the pressure between 1.0 atm and 0.97 atm to better represent physical laboratory conditions in the AFIT COAL Laboratory. This can be observed in Figure 33 and Figure 34.[5]

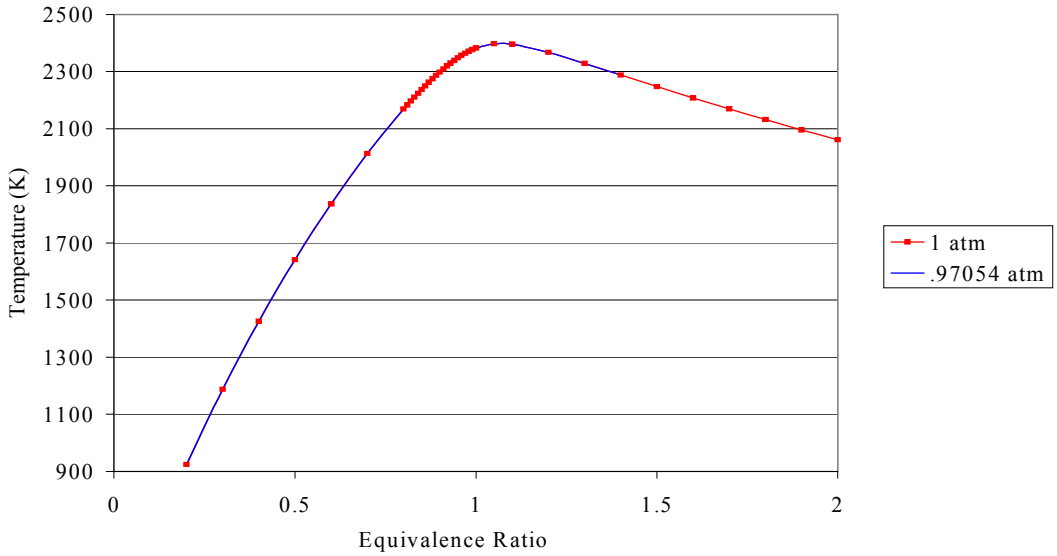

Figure 33: Theoretical equilibrium data - temperature vs. equivalence ratio[5]

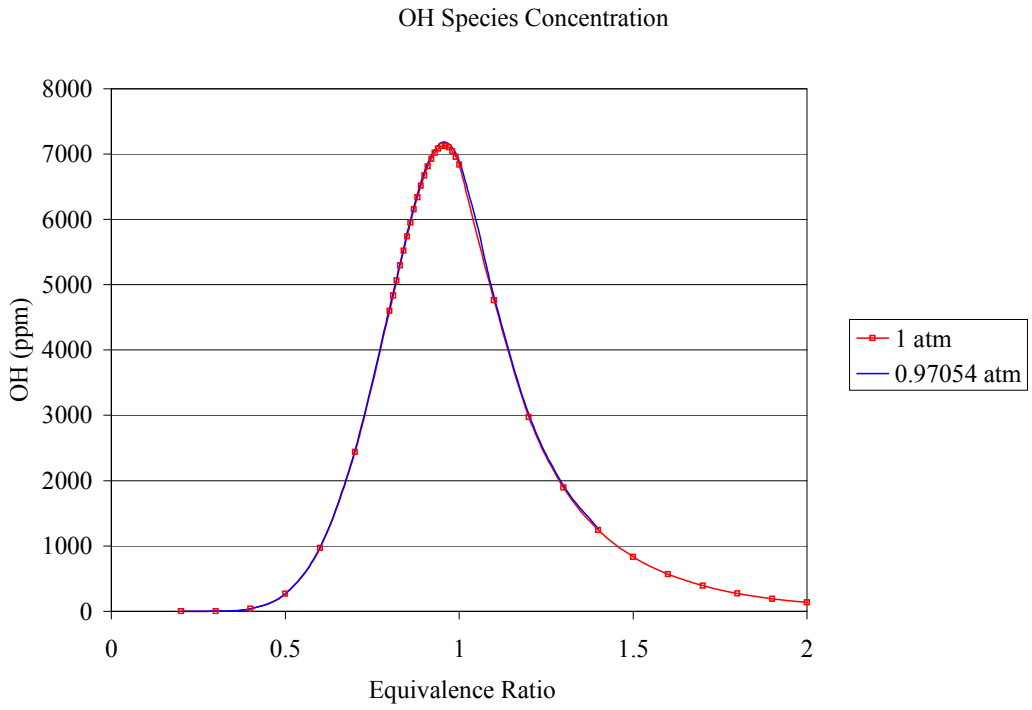

Figure 34: Theoretical equilibrium data - OH concentration vs. equivalence ratio[5]

Pressure for all calculations were assumed to be at 1.0 atm. Also presented in Hankins theoretical data is the adiabatic flame temperature was highest at $\Phi = 1.1$ and OH concentration was highest for $\Phi = 0.95$.

Collisional broadening effects for OH were calculated using CEA and plotted as shown in Figure 35.

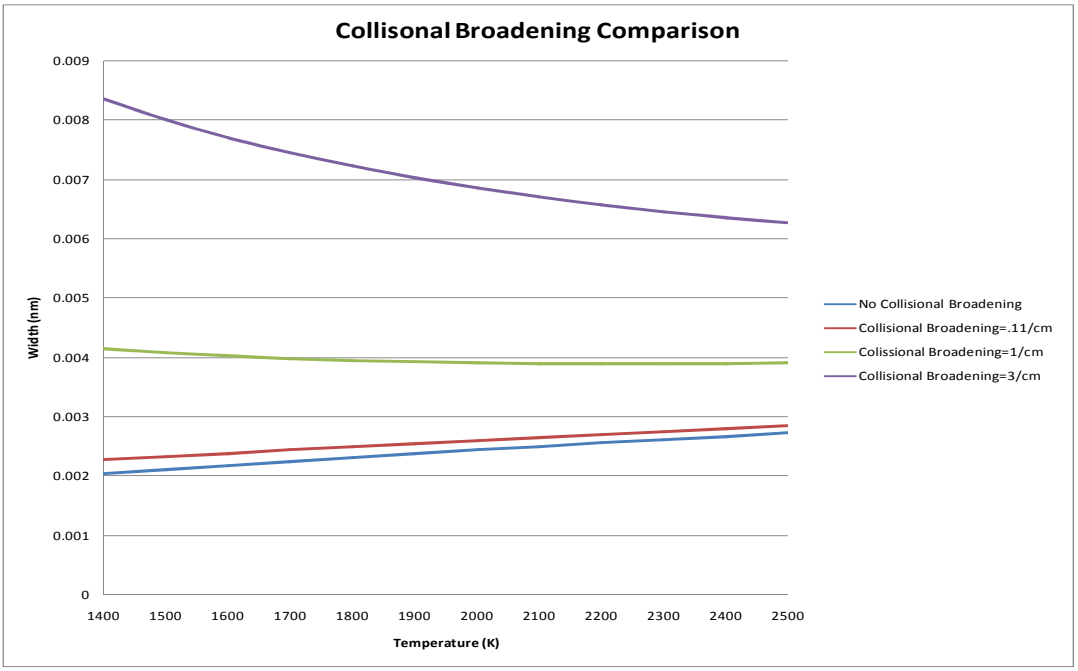

Figure 35: Collisional broadening comparison

The theoretical collisional broadening value for OH in this experiment is 0.11 cm^{-1}.[26] Other values were plotted to demonstrate the overall effect of collisional broadening on the data. For the conditions in this experiment, collisional broadening does not change the profile of the data, but merely shifts the data. As discussed in Chapter 3, the higher the temperature, the less effect collisional broadening has on the data, given the pressure

is maintained at roughly 1atm. When evaluating the raw data between no collisional broadening and a collisional broadening value of .11 cm^{-1} , there is an order of magnitude difference at the lower temperatures and a 1.5 orders of magnitude difference at the higher temperatures. Evaluating Figure 34, it is obvious that Doppler broadening clearly dominates, but one cannot ignore the fact that pressure broadening does have an effect on the data, however small it may seem.

Experimental data was gathered, reduced, and then compared to the theoretical data to ensure accuracy of the TDLAS system. It is important to note that theoretical data assumes complete combustion.

For a complete understanding of the results, basic data must first be assessed. As previously mentioned the data output from each scan is in the form of voltages and requires further reduction, calculation and analysis. Observing the behavior of one waveform gives an indication of viable or non-viable data was gathered. Figure 36shows time resolved raw data at $\Phi = 1$ for one wave form.

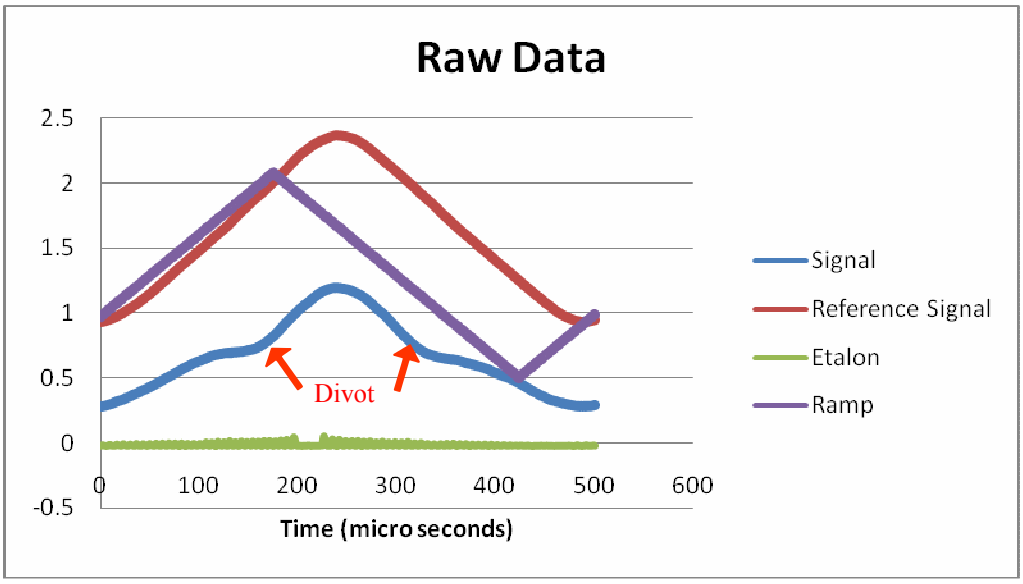

Figure 36: Time resolved raw data for one wave form at Φ=1

The signal in Figure 36 is the laser beam intensity after it has passed through the flame read by the photodiode. Reference signal is the 30 % split of the laser beam reading prior to passing through the flame and provides a base value for analysis of resultant data. The ramp is the power feed to the laser. The etalon is a tuning filter correlated to the absorption wavelength. The deficit in the etalon signal indicates the OH absorption wavelength. This is accomplished using the reference signal and the space between the peaks to ascertain the wavelength of the laser. This calculation is completed by an algorithm inherent in the VI. Only the "up ramp" etalon is plotted to avoid clutter. Observing the above results, the divot in the signal is a result of OH absorption at that time location in the scan. .

In Figure 36, there is a notable difference in peak location for the ramp and the reference and signal data. This is believed to be a result of a slight time lag due to the

path length of the data signal as well as some resistance that is inherent in the lab equipment. It is impossible to eliminate these two parameters, and therefore must be acknowledged. What was most important to consider was that the signal and reference peak locations occur simultaneously, otherwise, there would need to be significant investigation into reasoning behind the difference in these values. With this in mind, the two values were normalized and then plotted with one another in a time resolved fashion for consistency. This is shown in Figure 37.

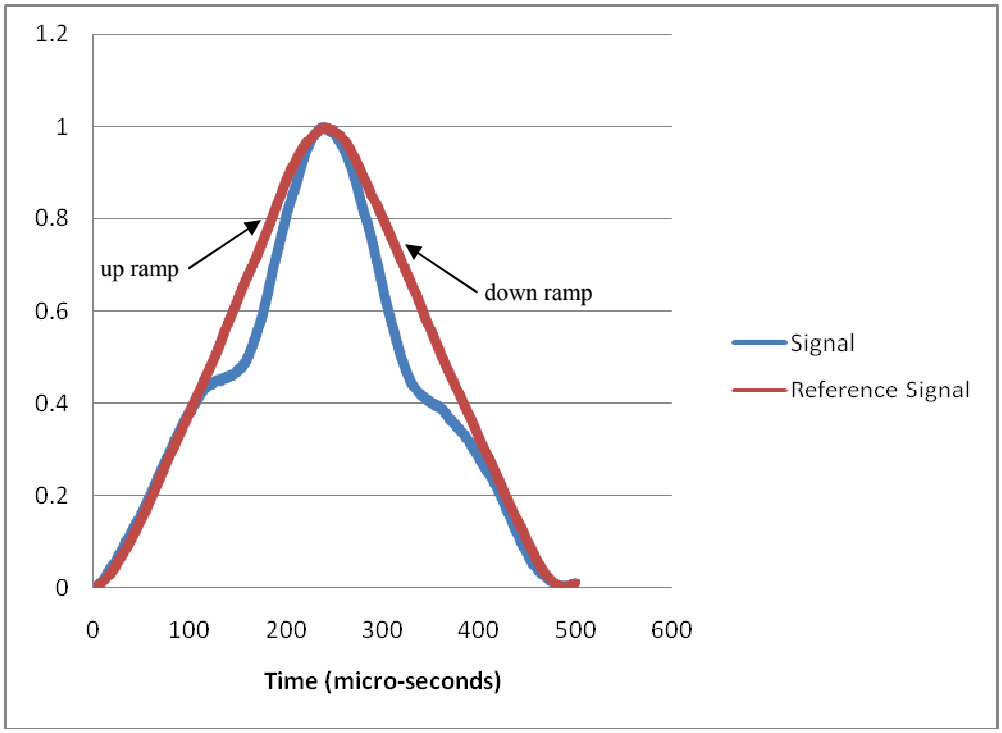

Figure 37: Comparison of normalized reference signal and absorption signal vs. time

We observe that the peak occurs at the same time location for both signals, and thus the reference signal may be used as a valid basis for calculating characteristics from

absorption data.

Noting that there are two absorption locations for each waveform, this begged a look at each ramp individually. The signal data was taken for one scan at an equivalence ratio of 1.0 for analysis. Each portion of the ramp was discerned by physically reviewing the data and finding a point in the data where the signal was the lowest. From this point, to a value where the signal was the highest was considered an "up ramp". From a highest value to a lowest value in succession was deemed "down ramp", essentially dividing the waveform in half to perform an analysis on one set of absorption signal data at a time. The data from the up and down ramps were also normalized and plotted against theoretical values calculated using LIFBASE, and can be seen in Figure 38 and Figure 39.

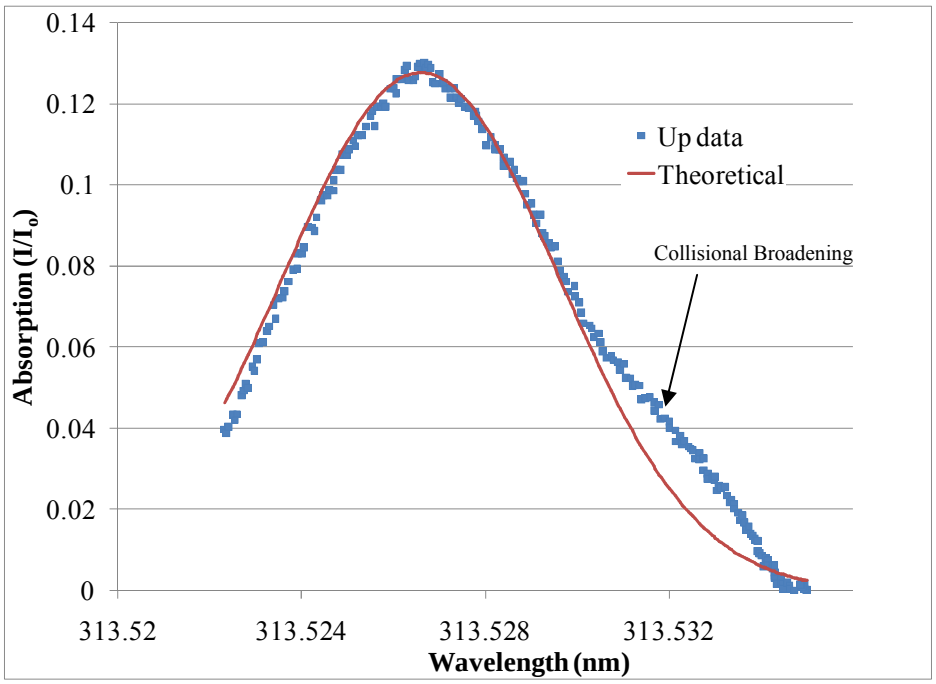

Figure 38: Up ramp signal data for the Hencken burner

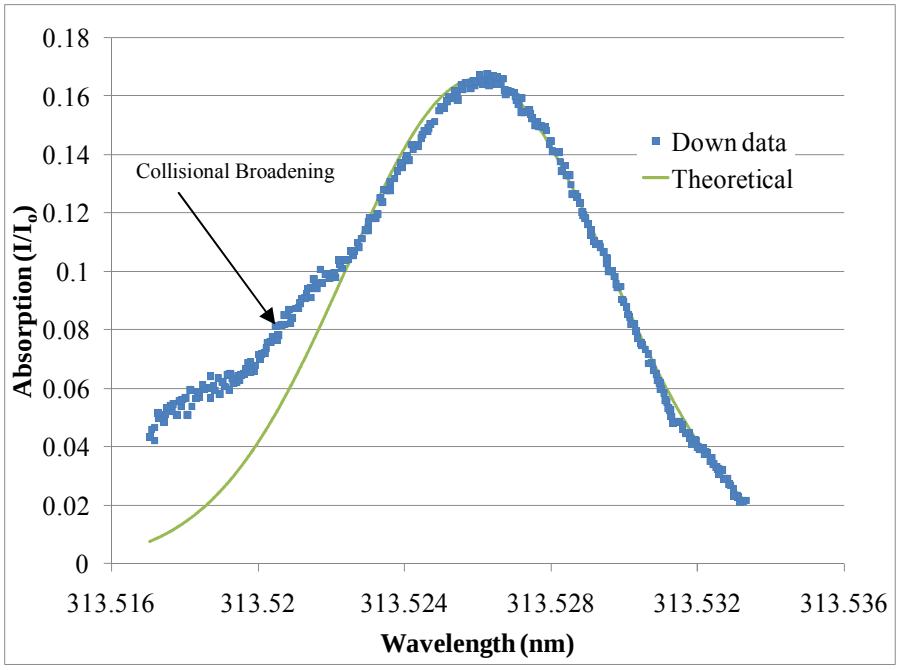

Figure 39: Down ramp signal data for the Hencken burner

The data from Figure 37 was separated into the up ramp and down ramp components. This was done as the spectroscopy technique used permits for a relationship between absorption and temperature and species concentration. The shape of the curve can be directly related to Doppler and collisional broadening. When both broadening effects are combined, the result is a Voigt profile. This is also refered to as a Lorentzian profile.

Observing the physical structure of the up and down ramps, attention is brought to the "wings" on each of them. This is collisional broadening present in the experimental data. The theoretical curve fit considers only the Gaussian shaped Doppler broadening, and thus does not match the Lorentzian portion of the data curve. This is not so much of a concern as, previously discussed, the collisional broadening does not present enough of an effect on the overall results. This is because the pressure at which the experiment was conducted was not sufficient for collisional broadening to have a dominant effect.[30] It is, however, prudent to recognize and acknowledge the presence of the collisional broadening in the data, as it is clearly present and noted in Figures 38 and 39. Since this is the case, the algorithm in the VI only considered Doppler broadening when calculating the theoretical curve fit. The theoretical values permit creation of a thermometer using the FWHM of the curve in relation to temperature.

Upon interpreting the above plots, it is noticed that the up ramp signal data is less noisy at the wing than the down ramp data. The absorption range was found to be

between 313.51nm and 313.53nm from Lab-View. This being the case, the up ramp signal provides better data along the theoretical curve than that of the down ramp for the frequency range.

4.1.2 Temperature Measurements

Several runs were made for each data set which corresponds to given equivalence ratios. Each set was taken at the same 2 cm above the surface of the burner and in the middle of the flame. The middle of the flame was considered to be half way in between the outer rows of N_2 ports and is 19mm from either outer edge of the grid on the Hencken Burner. This can be visually represented by the red arrow in Figure 40.

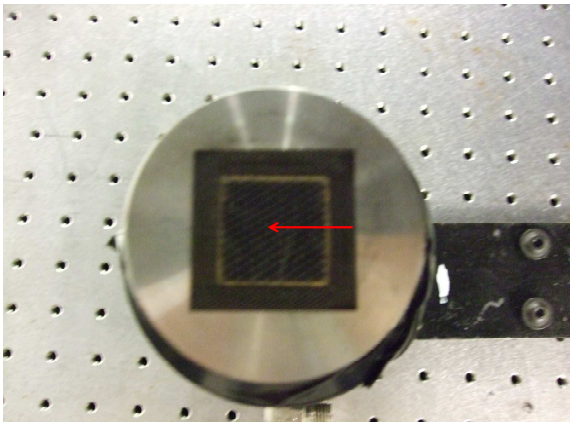

Figure 40: Laser path through Hencken flame

This particular location was chosen because it was convenient for set up and would be easily repeatable for future work. Five instances of data collection for each data set were performed in order to make the results statistically significant. The data

from each run was then averaged for the set and the resultant averaged data was then compared to theoretical values for analysis.

For comparative analysis to Meyer et al., as well as to demonstrate the temporal behavior of the temperature within the Hencken flame, a time resolved plot of temperature taken at Φ = 1 was created and is shown in Figure 41.

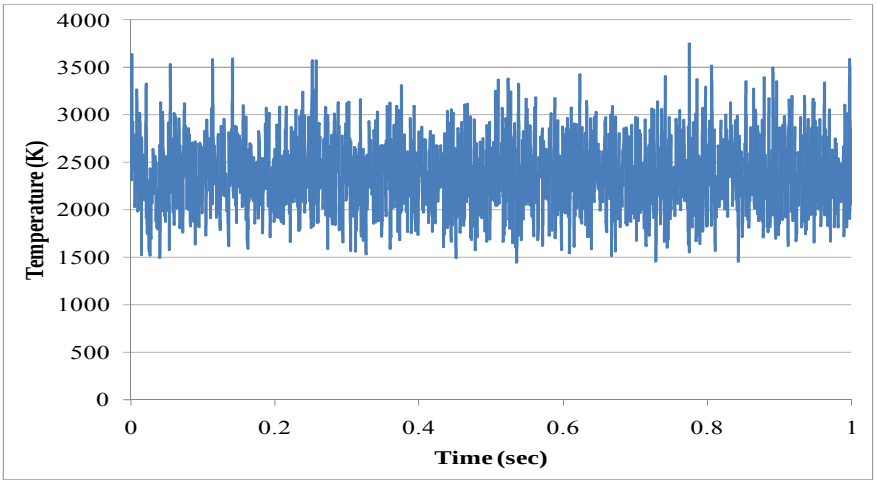

Figure 41: Time series of temperature for the Hencken burner at Φ=1

From previous research, the RMS of the temperature was taken at 2 kHz with an average temperature of approximately 2300 K.[25] The average temperature from the time series of this experiment seems to correlate well with these findings. Both up and down ramp data were included in the time series in Figure 41. Note the distinct bias shift between up and down ramp. This is attributed to the time lag in the electronics. For an additional perspective, a probability distribution function was calculated for the temperature range and appears below in Figure 42.

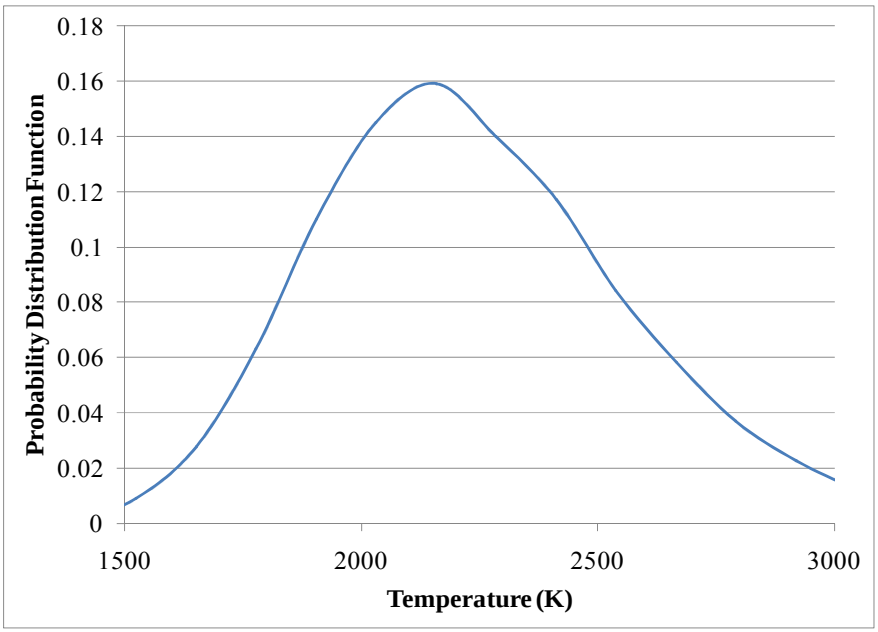

Figure 42: PDF of temporal temperature data for Hencken burner at Φ =1

Notice the two peaks in the PDF in Figure 42. This appears as two Gaussian distributions added together. This is further evidence of the time lag between the up and down ramp data. As such, the data was separated and calibrated individually.

Figure 42 suggests that the average temperature lays somewhere around 2200K rather than 2300K. This difference is most likely due to the fact that C_2H_4 was the fuel used for prior research and the fuel for this research is H_2.[27] The research from reference 27 was used for procedural and qualitative purposes.

As discussed in Chapter 3, temperatures were determined by obtaining the broadening of the signal and calculating the corresponding temperature using equation 11. Table 4 below shows the temperature calculations results of the upper and lower data sets as compared to theoretical CEA data.

Table 4: Temperature (K) results for a given Φ for experimental and theoretical data

Φ	T (up)	T (down)	T(CEA)
0.4	2.68E+03	3.34E+04	1425
0.5	6.27E+03	2.32E+04	1641
0.6	1.67E+04	4.29E+04	1836
0.7	5.08E+04	5.79E+04	2011
0.8	3.34E+04	5.08E+04	2165
0.9	3.60E+04	6.09E+04	2294
1.0	3.34E+04	4.81E+04	2378
1.1	3.90E+04	5.97E+04	2391
1.2	4.07E+04	4.04E+04	2363
1.3	1.96E+04	5.97E+04	2325
1.4	3.20E+04	4.55E+04	2284

A correlation factor is used because there is a variation in the experimental data versus the theoretical data. This was accomplished by taking the raw FWHM experimental data and dividing by the theoretical FWHM data. This was different for each equivalence ratio, but of significant note is that the equivalence ratios of 0.4-0.6 were outside reasonable limits and could not be correlated to theoretical data. Reasoning for this is most likely a result of low, and somewhat inconsistent, OH concentration due to lean fuel mixture.[27] This environment would not permit for adequate OH production to be present in the flame, and therefore instrumental readings would be affected. This error is then introduced into the resultant data and calculations. Table 5 shows the correlation factors for each Φ.

Table 5: Correlation Factors Between Experimental and Theoretical Data

Φ	**T (upper) Correlation Factor**	**T (lower) Correlation Factor**
0.4	1.557318	0.44124
0.5	1.092725	0.568217
0.6	0.708791	0.441952
0.7	0.425097	0.398192
0.8	0.543993	0.441075
0.9	0.539118	0.414738
1	0.570015	0.475013
1.1	0.528891	0.42745
1.2	0.514721	0.516512
1.3	0.735089	0.421477
1.4	0.571073	0.478874

Once these correlation factors were found, temperatures for experimental data were recalculated using MATLAB. The resultant experimental temperatures followed the trend of the theoretical temperatures relatively well and once the lower Φ values were eliminated from consideration, the temperature in the experimental data varied by as little as 1.5% and only as high as 6.5%. The results are shown in Figure 42.

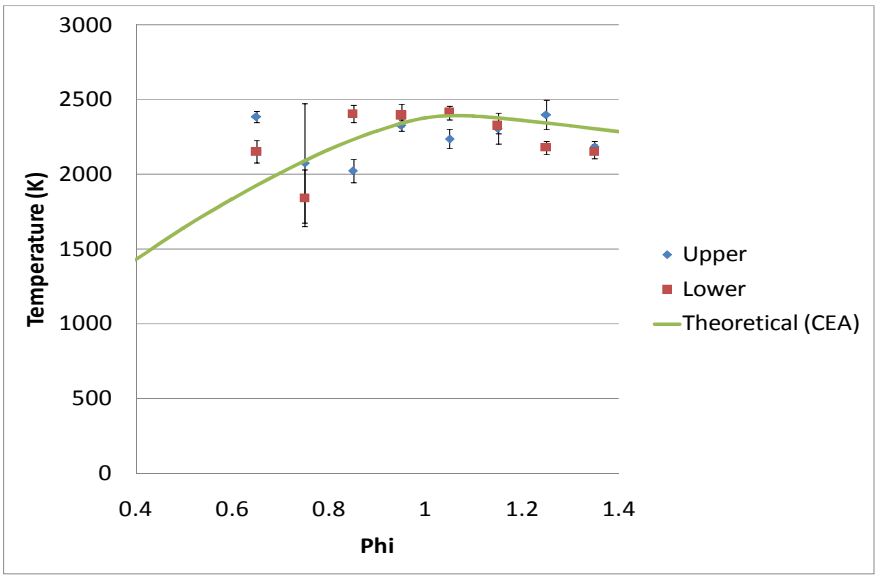

Figure 43: Experimental and theoretical flame temperatures

According to theoretical results, the highest temperature should have occurred at Φ=1.1; however this did not occur in the experimental data. There are several reasons for this occurrence. First, the measurements were taken at 20 mm above the burner surface. Recommendations from reference 27 are that measurements should be taken from 5-10 mm above the burner surface for best results. The mixing layer between the flame and co-flow increases the higher in flame one goes. This is entrainment of the co-flow, which is the mixing of cooler air, and results in a decrease of flame temperature. A warning exists that this situation creates a low temperature zone and the data must be interpreted carefully.[27] Further, it was noted that data taken beyond 10 mm from the burner surface shows a decline in temperature due to radiation heat losses from combustion products.[25] Second, the theoretical data results assume equilibrium combustion in adiabatic

conditions. The Hencken flame is not adiabatic nor does chemical equilibrium occur, suggesting there is heat loss due to radiation, conduction, and unburned fuel.

4.1.3 OH Concentration Measurements

As discussed earlier, concentration measurements are calculated from line broadening. Both the line width and the concentrations were calculated for experimental data and compared to theoretical data for assessment. A temporal representation of OH concentration taken at Φ = 1 is presented for comparison and analysis and is shown in Figure 44.

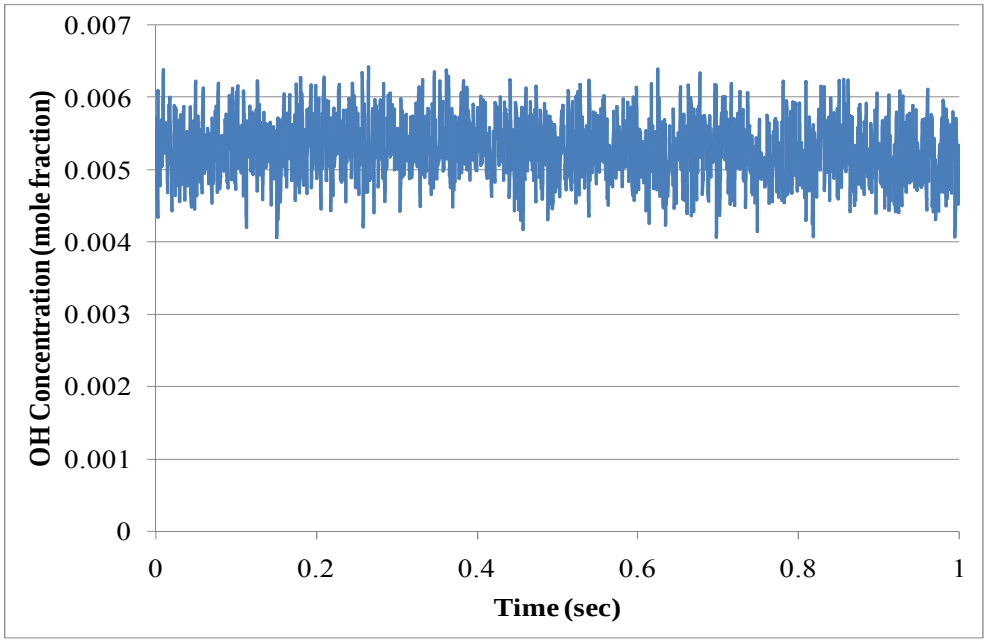

Figure 44: Time series of OH mole fraction for Hencken burner at Φ=1

Data taken at 2 kHz and at 15 mm above the center of the burner surface shows an OH mole fraction average of about 4300 ppm for ethylene.[27] The experimental data for

this research was also taken at 2 kHz, but was at a vertical distance of 20 mm above the burner surface and for hydrogen fuel. The average for the data in this experiment is roughly 5100 ppm.

Evaluation of experimental against theoretical data need to be made to assess the accuracy of the measurements. Figure 45 shows the concentration comparison.

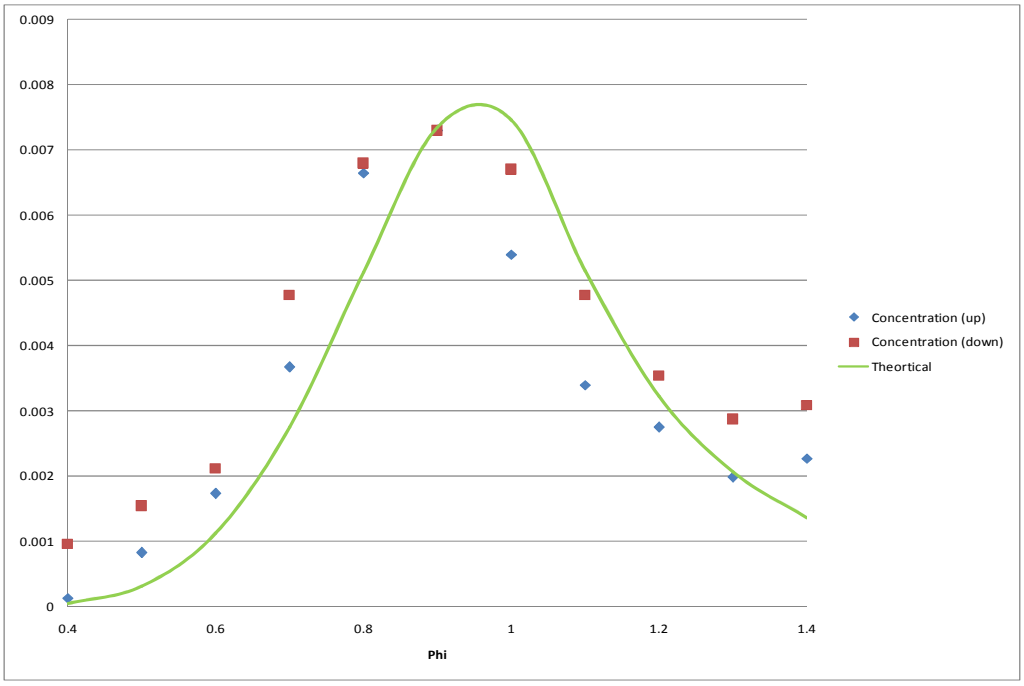

Figure 45: OH concentration for Hencken flame

It is stated in reference 27 that though taking measurements too far from the surface will affect temperature results, absorption measurements taken higher in the flame at wider mixing layers will still yield accurate results. Observing the above data, the experimental results clearly follow the same trend as the theoretical results, only shifted to the left. After careful analysis, it was determined that the horizontal shift was

exactly a factor of 0.5 at every data location and was embedded in the equivalence ratio. Table 6 shows the experimental and theoretical calculated concentrations for each equivalence ratio. Data is not reliable for equivalence ratios from 0.45-0.65 for the same reason as in the temperature calculations.

Table 6: OH Concentration calculation for Hencken flame

Φ	**CEA**	**Concentration (U)**	**Concentration (D)**
0.45	0.00005	0.000131394	0.000957
0.55	0.00031	0.000822261	0.001544
0.65	0.00112	0.001731226	0.002112
0.75	0.00275	0.003665608	0.004772
0.85	0.00512	0.006648578	0.006793
0.95	0.00735	0.007295738	0.007297
1.05	0.00746	0.005400764	0.006702
1.15	0.00515	0.003396187	0.00477
1.25	0.00322	0.002747302	0.003536
1.35	0.00206	0.001979835	0.002872
1.45	0.00136	0.002272387	0.003084

Once the correction was made, the resultant data was once again compared to theoretical data. This is illustrated below in Figure 46.

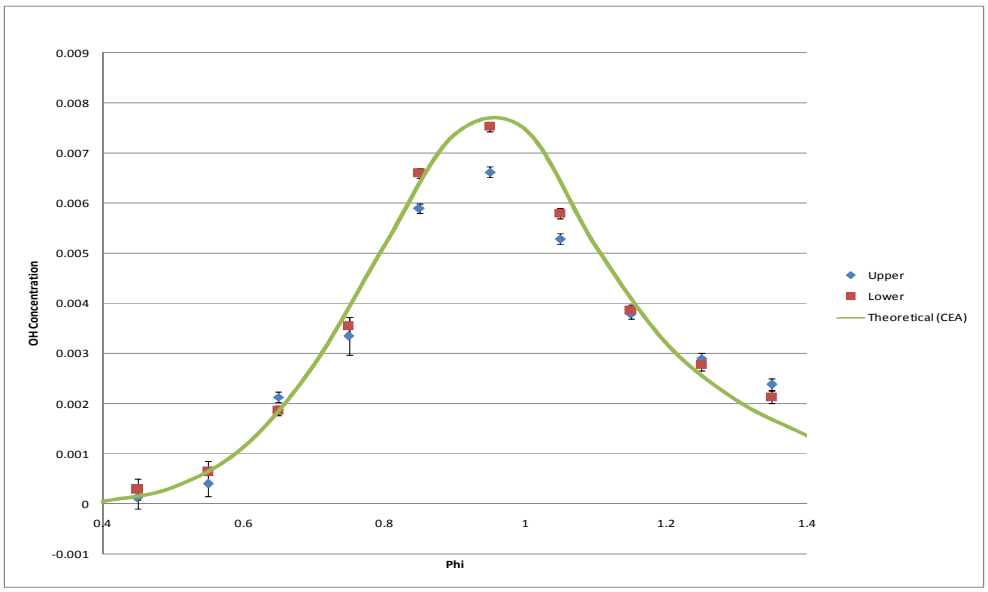

Figure 46: OH concentration for Hencken flame with Φ correction

Theoretical results state that peak concentration should occur at Φ= 0.95. This is indeed the case for the experimental data with the correction. However, the magnitude of the experimental concentration does not match that of the theoretical data. A factor was calculated that would quantify the difference between the theoretical and experimental data. This was accomplished by minimizing the square of the differences between the two values. Table 7 shows the calculated factors for each Φ.

Table 7: Correlation factor for experimental and theoretical data

Φ	Factor (U)	Factor (D)
0.45	6.65E-01	1.89E-01
0.55	4.64E-01	2.41E-01
0.65	2.99E-01	1.87E-01
0.75	1.79E-01	1.68E-01
0.85	2.28E-01	1.85E-01
0.95	2.25E-01	1.73E-01
1.05	2.24E-01	1.94E-01

1.15	2.20E-01	1.78E-01
1.25	2.15E-01	2.16E-01
1.35	2.62E-01	1.42E-01
1.45	2.13E-01	1.65E-01

Other than the obvious anomalies at low equivalence ratios, the correlation factor is relatively constant. This can be visualized in Figure 47

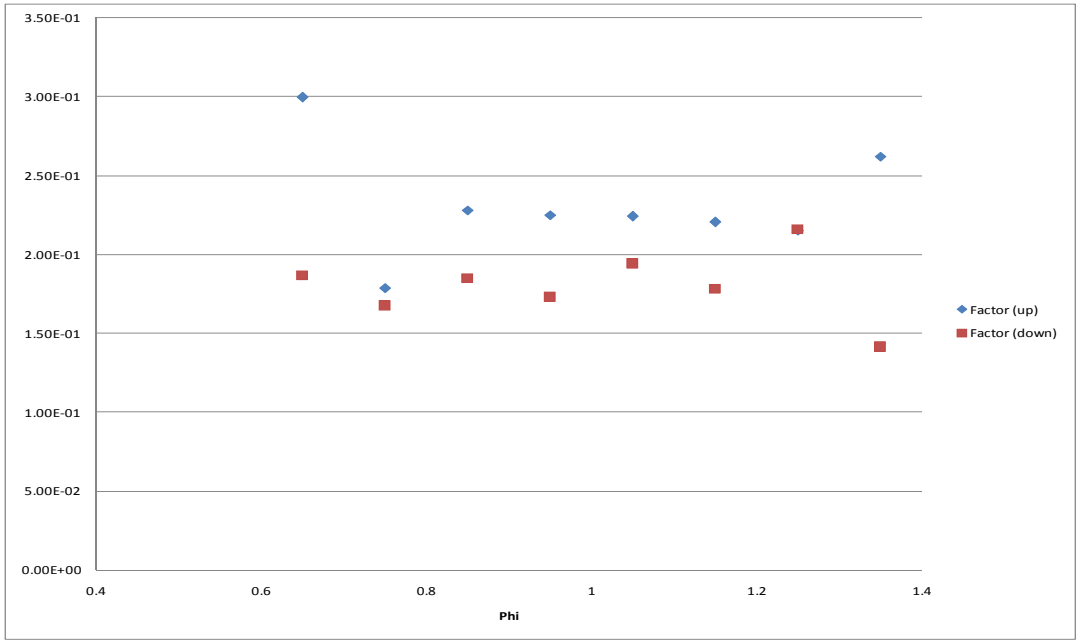

Figure 47: Correlation factor of theoretical and experimental data

The correlation factor hovers around an average value of approximately 0.22. The fact that this factor is fairly constant suggests that there may exist some sort of bias in the system instrumentation. Another consideration is that these measurements were reduced and calculated with Doppler broadening effects only. Collisional broadening was not considered and therefore will introduce slight error into the results. With these factors

taken into consideration, the concentration data only varied by 7.2% at most from theoretical data.

4.2 TDLAS Jet Diffusion Flame Measurements

The jet flame used for this analysis was a 50/50 mix of ethylene and nitrogen. Measurements for varying Reynolds number were taken at the centerline of the jet and twenty diameters above the outlet. This was to ensure the data was taken in the fully developed flame area. Once the data was obtained for a set range of Reynolds numbers, the beam was traversed horizontally from the centerline to the outer flame edge. Data was collected and reduced. From the analysis of the Hencken burner, correlation factors were established. The actual calculation occurred in a Matlab script.

4.2.1 Centerline Temperature Measurements

Reynolds number was varied from 1000-5750 to compare the laminar to turbulent regime for the jet diffusion flame. Temperature measurements at the centerline of the jet for varying Re are shown in Figure 48.

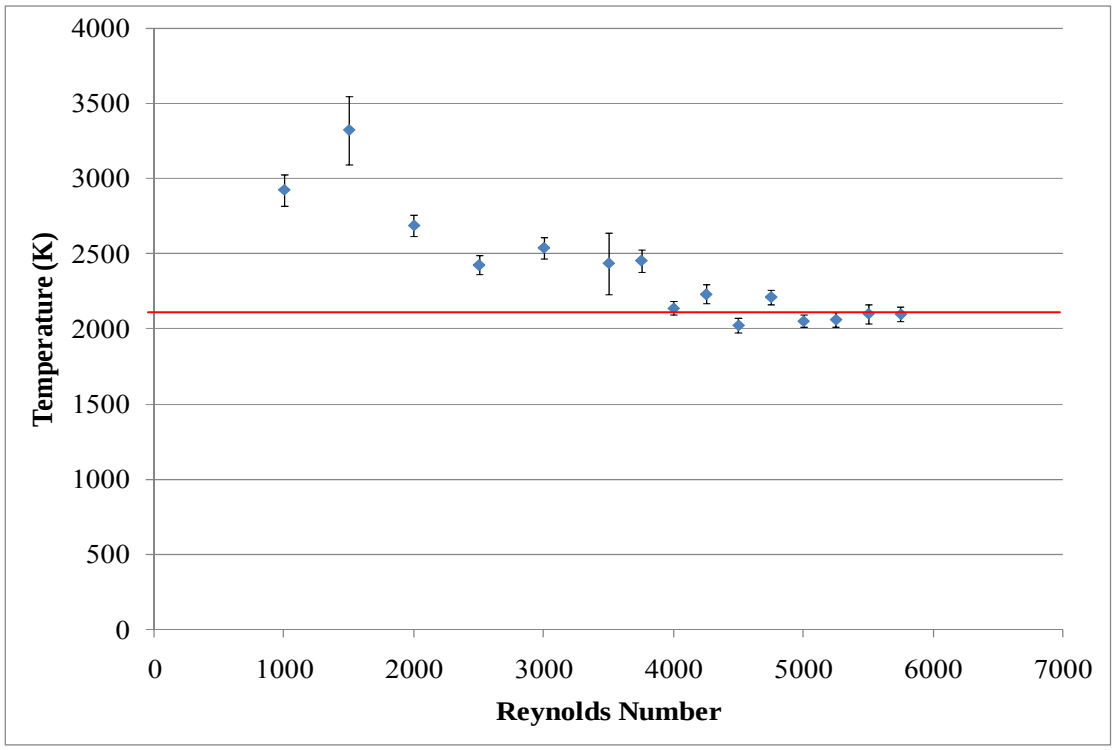

Figure 48: Temperature measurements at centerline of jet flame

The horizontal red line in Figure 48 denotes the adiabatic flame temperature of approximately 2250 K. Notice there is a decreasing trend for increasing Reynolds number at this location for data collection. Further, the turbulent nature of the flame contributes significantly toward this trend. At lower Reynolds numbers, the length scale of turbulence is much larger, creating larger fluctuation intensities.[38] This results in inaccurate temperatures primarily due to the intermittency of the flame flickering in and out of the measurement volume. When the Reynolds number is increased, the length scale becomes smaller and the fluctuation intensity is not as pronounced, resulting in a

more consistent flame structure in the measurement volume, and thus a more consistent temperature reading. [38] Since the data collected is as a path averaged signal, it includes all of the fluctuations. These fluctuations are introduced and evident in the data. It is important to note that the VI does not take into account the quality of the data. The VI forcefully fits a Gaussian curve to all data, therefore the average width of the curve is wider and shorted that theoretical calculations. This produces artificially high temperatures and lower OH concentrations. An interesting observation was made for the behavior of the data. Liftoff occurred at Re = 3500 and temperature fluctuations were less intense and were close to the adiabatic flame temperature. Note the larger fluctuation in the temperature readings prior to liftoff

As discussed the inherent variation in the data is a result of the turbulent nature of the flame. Turbulent intensity was calculated and the results are show in Figure 49.

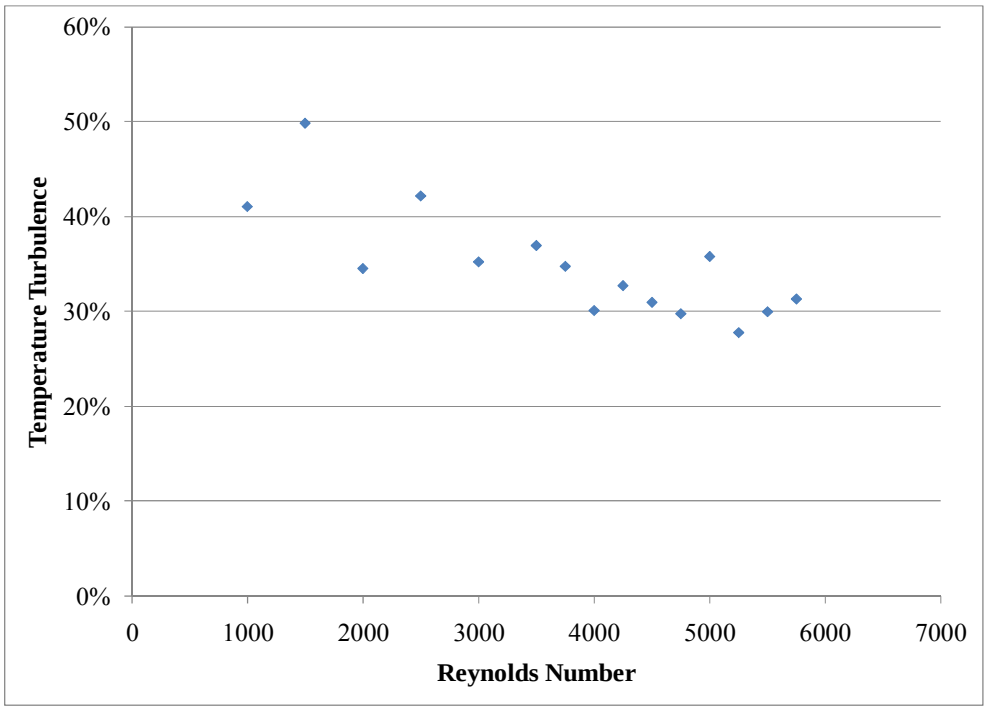

Figure 49: Temperature turbulent percentage for jet flame

The overall trend is that of a decreasing percentage of temperature turbulence with increasing Reynolds number. Again, the turbulent length scales are at play. As turbulence increases, the scales decrease. Turbulent intensity is still quite high. Consideration must be given that this flow is also reacting, and chemical kinetics are contributing to the variation and fluctuation in the flame environment. Since the scans are an average over this entire area, even uncharacteristic fluctuations in the flow will propagate into the data results. This can create difficulties when trying to interpret results for an inhomogeneous, unsteady environment.

4.2.2 Centerline OH Concentration Measurements

The same calculations were completed for concentration measurements of OH and are presented in Figure 50.

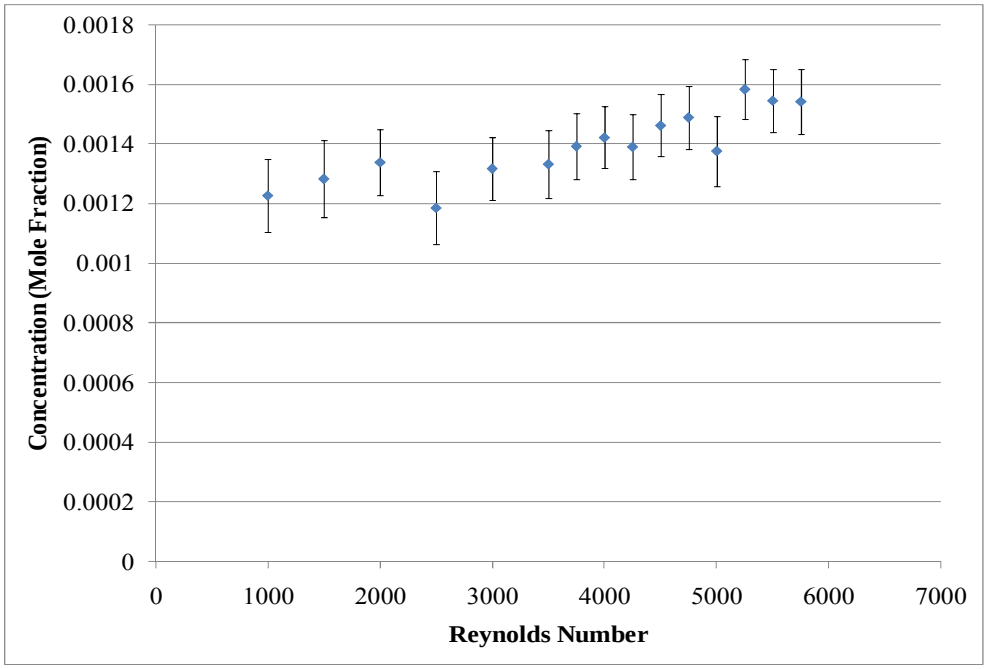

Figure 50: Concentration measurements at centerline of jet

The concentration trend increases with increasing Reynolds number of the jet flow. This once again can be explained by the turbulent length scales. As the length scales are larger, fluctuations in the actual flame itself are much more pronounced. This "flickering can create areas where the laser beam is not reading a portion of the flame at all. As the turbulence increases with Reynolds number, the flickering is more compact and the data collected contains a larger amount of actual flame readings. Another consideration is the diffusive nature of the jet. As the jet diffuses, there is a larger

amount of fuel introduced for mixture with air, and thus more burning. Both explanations require further data analysis for verification, and can be the basis for future research.

The inherent variable nature of the data for a turbulent regime is once again analyzed for OH concentration in terms of turbulent intensity. This percentage was determined in the same fashion as that of temperature previously discussed, and is presented in Figure 51.

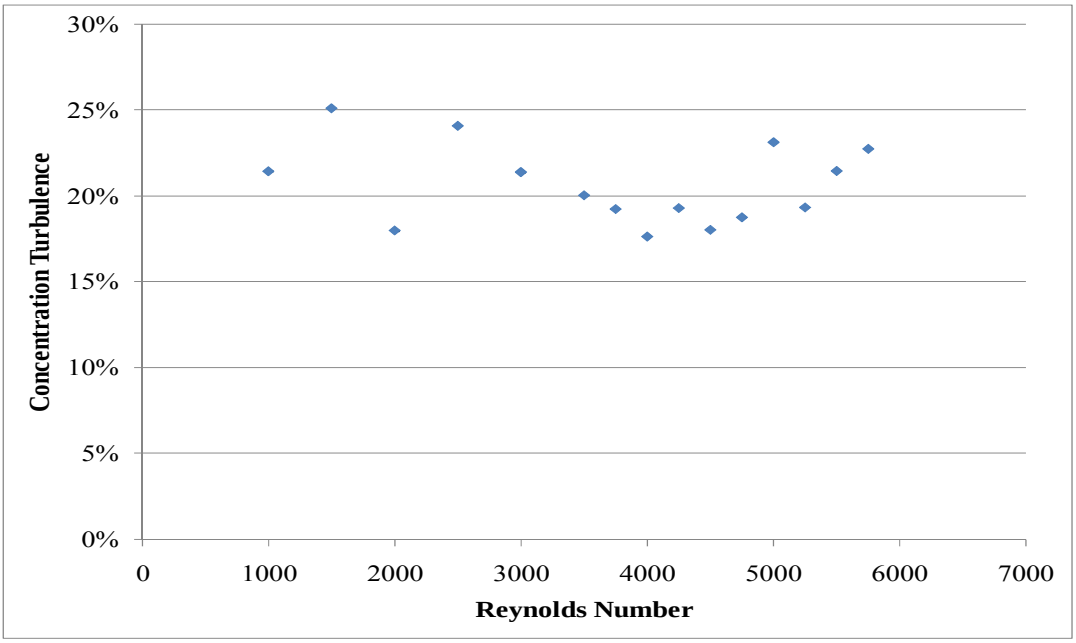

Figure 51: OH concentration turbulent percentage for jet flame

The turbulent concentration trend of OH for the turbulent jet flame further verifies the concentration results for the same basis of reasoning. As the Re is increased, fluctuations intensities decrease, the area of the diffusion jet increases, and there is more

OH concentration in each data scan. As previously mentioned, reacting flow is more turbulent than a non reacting flow. More fuel is introduced, and thus more reaction is taking place, insomuch as the flow characteristics are below blow out levels.

Turbulent concentration below liftoff of Re = 3500 is highly irregular and most likely due to intense turbulent fluctuations. Path averaging makes it difficult to analyze these readings and therefore conclusions are hard to make for the data in this range. Notice at liftoff, turbulent intensity increases with Re, as expected. This is a result of the flame structure change, as previously discussed. The more structured the flame, the more data is captured in the measurement volume, giving a much more accurate reading. This demonstrates that the instruments can capture flame liftoff.

4.2.3 Traversed Measurements

Once centerline data was gathered, the Re was kept at a constant value of 5750. The beam was then traversed from the centerline of the flame to the edge in increments of 0.5 mm up to 3.0 mm from centerline, where increments were then increased by 1 mm to a maximum of 18 mm from centerline. Temperature data for the traversed location was calculated and is presented in Figure 52.

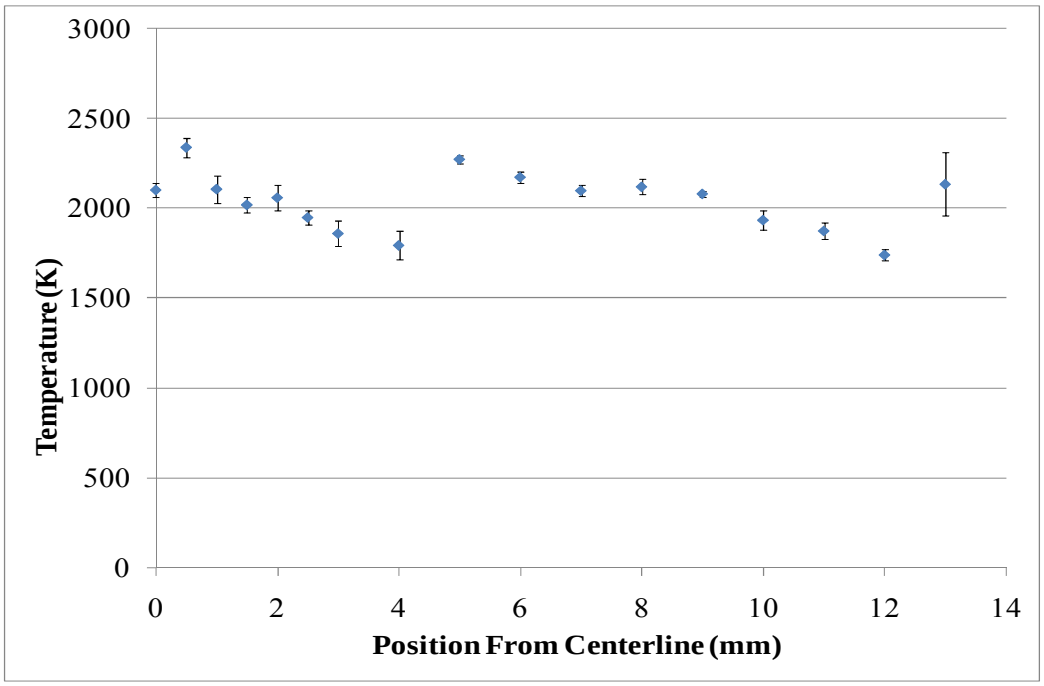

Figure 52: Temperature values per flame location from centerline for jet flame, Re=5750

In observing the behavior of temperature with respect to position, temperature suddenly increases between the 4 and 5 mm traversed positions. There is approximately a 500 K increase in temperature. This is due to the physical nature of the jet flame. If it were possible to slice a flame horizontally and look at the profile from the top, one would see a region in the center where no burning is taking place.[37] Only hot gases that have yet to combust are present. As the jet diffuses outward, a more ideal mixture of fuel and oxidizer occurs and combustion takes place. As such, the increase in temperature between the 4mm and 5mm position can be explained at the location of the interface of the non-burning center area of gas with outer reacting area, or flame interface. Also noteworthy is the downward trend of temperature after this flame interface. From flame

structure theory, as diffusion of the fuel occurs, it mixes with ambient air. As this occurs, the flame propagates through this diffusive mixture to the point where the fuel oxidizer mixture is too lean to sustain burning. This is the outer edge of the flame, or the flame front. As such, temperature will be lower in this fuel lean environment.

This can be further verified by observing the concentration measurements with respect to location shown in Figure 53.

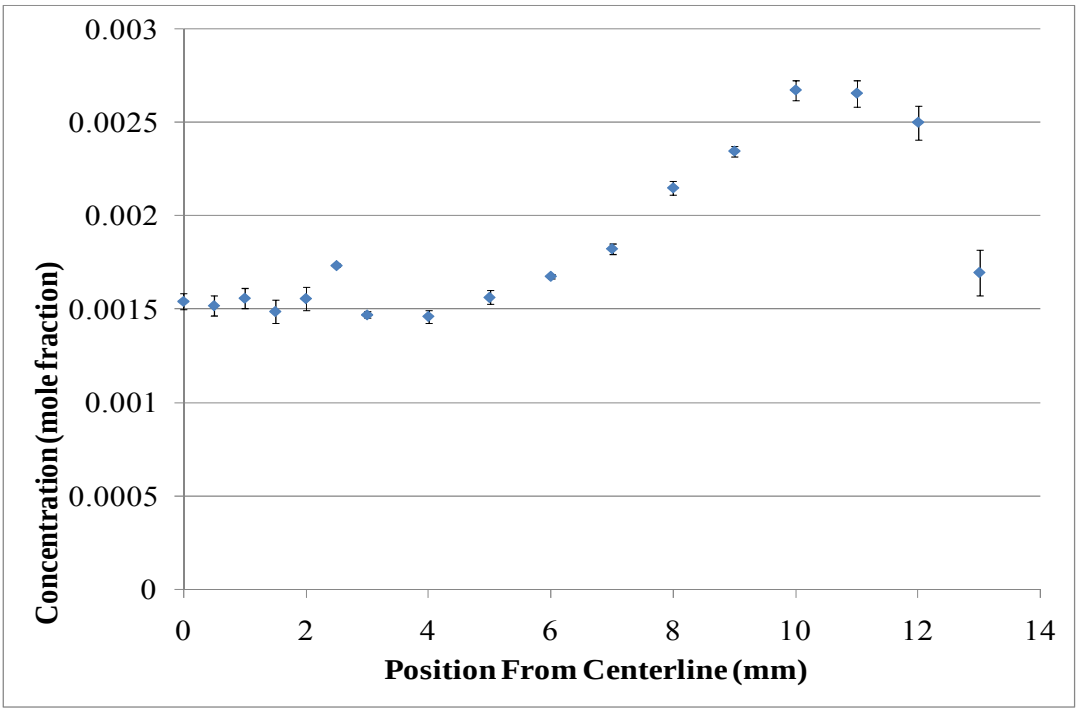

Figure 53: OH concentration values per flame location from centerline for jet flame

The increase in concentration begins in the same location as the sudden increase in temperature, further verifying the location of the flame interface with the non-reacting center. As combustion occurs, OH is produced.

Of further interest is that OH production peaks and falls off. This further verifies the previous explanation of the temperature profile and its correlation to theory. OH will be produced so long as combustion is occurring. Note the trend from the 0 position to the 4mm position is relatively flat, indicating minimal OH production. Upon rise in temperature, and hence flame interface location, the production of OH increases. Further, OH production peaks and falls off almost to the same concentration reading as the non-burning center of the flame. This indicates the flame front. The same logic applies as given in the explanation of the temperature profile. Both temperature and concentration results correspond well with flame theory.

As with the centerline measurements, turbulent concentration for both temperature and concentration were considered. Given the inverse relationship discussed for the temperature and concentration turbulent percentages, it was decided to plot these values together for analysis. This is illustrated in Figure 54.

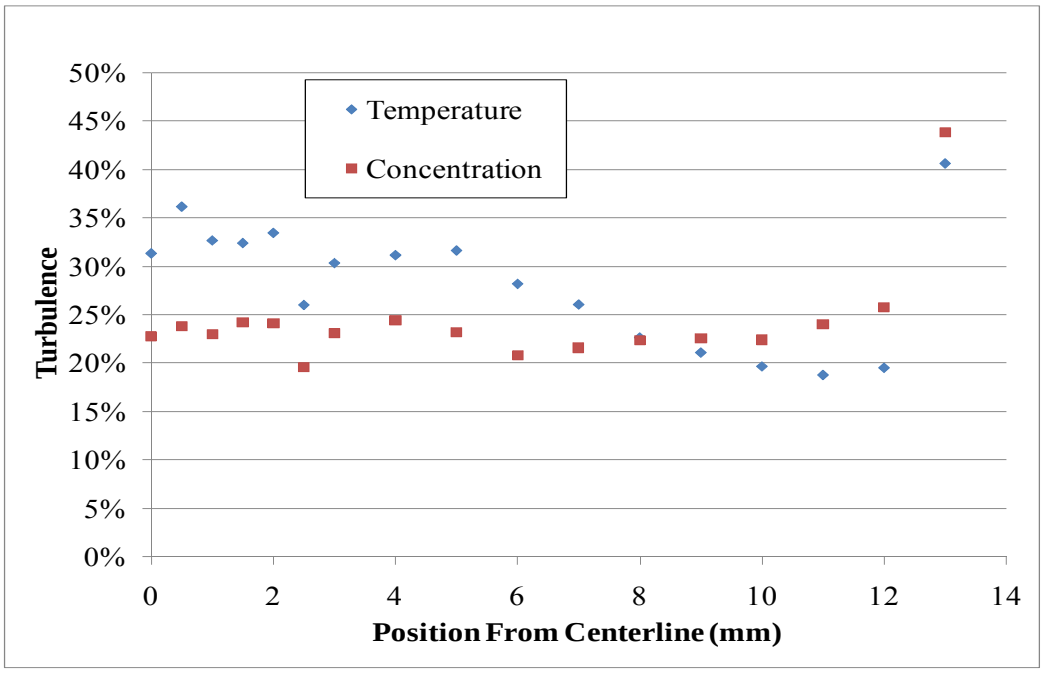

Figure 54: Traversed temperature and OH concentration turbulent percentages for jet flame

From temperature and concentration profiles, it was determined that the flame interface was located at approximately 4 mm from the flame centerline. The data shows no real trend for the turbulent percentages prior to the 4 mm location. Once in the flame, the data show a clear trend for both parameters.

5 Conclusions and Recommendations

5.1 Laser Diagnostics

The AFIT COAL laboratory is now equipped with an operational TDLAS system for further testing on the UCC. The system has been validated by a laminar flame produced by a Hencken burner and is set up to perform OH absorption spectroscopy. Concentration and temperature measurements have been taken and verified by comparison with theoretical data as well as previous research. It is recommended that data be taken within the 5-10 mm vertical range above the surface of the burner for more accurate temperature readings when using the TDLAS system. This may alleviate any difficulties in data analysis as well as provide for a better correlation with established experimental results. Furthermore, it was found that this data would be ideal for application of an Abel transform. This would allow for calculation of concentrations and temperatures as a function of radius. Utilizing the Abel transform approach would produce actual flame statistics rather than the path averaged results obtained in this thesis.

Further verification of the system for a turbulent environment was carried out. As discussed, the TDLAS system gave indications of flame interface and flame front. Data results correlate very well with turbulent jet flame theory. Data results indicate usefulness of this system for determining flame location, flame thickness, species concentrations, as well as other performance parameters. This provides another tool for achievement of the UCC research objectives.

5.2 Future Work

Several modifications to the COAL laboratory are recommended. The optics table set up in relation to the combustion rig is very inconvenient and becomes increasingly difficult to navigate. Relocation of the rig closer to the back wall is recommended.

With the verification of the TDLAS system now complete, the optics tables are becoming increasingly full. It is recommended that a reconfiguration study of the optics tables for maximum efficiency be carried out and additional optics tables be added to the configuration as needed.

Experimentation on the UCC with TDLAS is now ready to commence. Analysis on the infinite radius section as well as the curved section can be accomplished. OH concentrations and temperatures can be calculated. Furthermore, these parameters can be used for flame location as well as correlated to efficiencies for the UCC. These results can be compared to data collected using several other methods of interrogation for a complete and thorough analysis of the UCC behavior.

Turbulent analysis of the TDLAS system results requires further processing and provides a good basis for future work. Given the path averaging nature of the system, it is further recommended that the TDLAS be used in conjunction with other spectroscopic tools for a more in depth analysis of future combustion experiments.

Bibliography

1 AIAA Position Paper, "Versatile Affordable Advanced Turbine Engines (VAATE) Initiative," January 2006.

2 Moenter, D. S. *Design and Numerical Simulation of Two-Dimensional Ultra-Compact Combustor Model Sections for Experimental Observation of Cavity-Vane Flow Interactions.* MS Thesis, AFIT/GAE/ENY/06-S07. Graduate School of Engineering and Management, Air Force Institute of Technology (AU), Wright-Patterson AFB, OH, September 2006.

3. AIAA Position Paper, "Versatile Affordable Advanced Turbine Engines (VAATE) Initiative," *AIAA Air Breathing Propulsion Technical Committee*, Reston, VA, January 2006.

4. Hancock, R. D., Bertagnolli, K. E., Lucht, R. P. Nitrogen and Hydrogen CARS Temperature Measurements in a Hydrogen / Air Flame Using a Near-Adiabatic Flat-Flame Burner. *Combustion and Flame 109, pp. 323-331*. 1997

5. Hankins, Terry. *Laser Diagnostic System Validation and Ultra-Compact Combustor Characterization*. MS thesis, AFIT/GAE/ENY/08-M14. Graduate School of Engineering and Management, Air Force Institute of Technology (AU), Wright-Patterson AFB OH, March 2008

6 Lakusta, Patrick, *Laser Diagnostic System Validation and Ultra-Compact Combustor Characterization*. MS thesis, AFIT/GAE/ENY/08-M14. Graduate School of Engineering and Management, Air Force Institute of Technology (AU), Wright-Patterson AFB OH, March 2008

7 Turns, S. R. *An Introduction to Combustion* (2nd Ed.). New York: McGraw-Hill, Inc., 1996.

8 Glassman, Irvin. *Combustion*(3rd Ed.). San Diego, California; Academic Press, 1996

9 Oats, G.C. Aerothermodynamics of Gas Turbine and rocket Propulsion, 3rd ed, American Institute of Aeronautics and Astronautics, Inc.

10 Society of Automotive Engineers, Inc., "Aerospace Recommended Practice: Procedure for the Analysis and Evaluation of Gaseous Emissions from Aircraft Engines." ARP1533, Warrendale, PA: 2004.

11 Mattingly, J. D. *Elements of Gas Turbine Propulsion.* New York: McGraw-Hill, Inc., 1996.

12 Zelina, J., Sturgess, G.J., Shouse, D. T., "The Behavior of an Ultra-Compact Combustor (UCC) Based On Centrifugally-Enhanced Turbulent Burning Rates," *40th AIAA/SAE/ASME/ASEE Joint Propulsion Conference & Exhibit,* AIAA-2004-3541, Fort Lauderdale, FL, July 2004.

13 Greenwood, R. T. *Numerical Analysis and Optimization of the Ultra-Compact Combustor.* MS thesis, AFIT/GAE/ENY/05-M10. Graduate School of Engineering and Management, Air Force Institute of Technology (AU), Wright-Patterson AFB OH, March 2005.

14 Lewis, G. D., "Centrifugal-Force Effects on Combustion," *14th Symposium (International) on Combustion,* The Combustion Institute, pp.413-419, 1973.

15 Anthenien, R. A., Mantz, R.A., Roquemore, W.M., & Sturgess, G. "Experiemental Results for a Novel, High Swirl, Ultra-Compact Combustor for Gas Turbine Engines," 2nd Joint Meeting of the United States Section of the Combustion Institute, Oakland, CA. 2001.

16 Zelina, J., Sturgess, G.J., Shouse, D. T., "The Behavior of an Ultra-Compact Combustor (UCC) Based On Centrifugally-Enhanced Turbulent Burning Rates," *40th AIAA/SAE/ASME/ASEE Joint Propulsion Conference & Exhibit,* AIAA-2004-3541, Fort Lauderdale, FL, July 2004.

17 Sirignano, W. A., and Liu, F., "Performance Increases for Gas-Turbine Engines Through Combustion Inside the Turbine," *Journal of Propulsion and Power,* 15:1 pp.111-118, 1999.

18 (Little et al., 1979).

19 Hsu, K-Y, and Goss, L. P., "Characteristics of a Trapped-Vortex Combustor," *Journal of Propulsion and Power,* Vol. 14, No. 1, 1998.

20 Roquermore, W. M., Shouse, D., and Burrus, D., "Trapped Vortex Combustor Concept of Gas Turbine Engines," *39th AIAA Aerospace Sciences Meeting & Exhibit,* AIAA 2001-0483, Reno, NV, January 2001.

21 Yonezawa, Y., Toh, H., Goto, S., and Obata, M., "Development of the Jet-Swirl High Loading Combustor," *26th AIAA/SAE/ASME/ASEE Joint Propulsion Conference,* Orlando, FL, AIAA-90-2451, Orlando, FL, March 1990.

22 Sirignano, W. A., and Liu, F., "Performance Increases for Gas-Turbine Engines Through Combustion Inside the Turbine," *Journal of Propulsion and Power,* 15:1 pp.111-118, 1999.
23 Liu, F., and Sirignano, W. A., "Turbojet and Turbofan Engine Performance Increases Through Turbine Burners," *38th Aerospace Sciences Meeting & Exhibit*, AIAA-2000-0741, Reno, NV, January 2000.
24 Kohse-Hoinghaus, K., and Jefferies, J. *Applied Combustion Diagnostics.* New York, NY: Taylor & Francis, 2002.
25 Giezendanner-Thoben, R., Meier, U., Meier, W., Heinze, J., Aigner, M., "Phase-locked two-line OH planar laser-induced fluorescence thermometry in a pulsating gas turbine model combustor at atmospheric pressure," Applied Optics, Vol. 44, No. 31, November 2005.
26 Anderson, W. S. *Design, Construction, and Validation of the AFIT Small Scale Combustion Facility and Sectional Model of the Ultra-compact Combustor.* MS thesis, AFIT/GAE/ENY/07-M01. Graduate School of Engineering and Management, Air Force Institute of Technology (AU), Wright-Patterson AFB OH, March 2007.
27 Hankins, T. *Laser Diagnositic System Validation And Ultra-Compact Combustor Characterization*. MS thesis, AFIT/GAE/ENY/08-M15. Graduate School of Engineering and Management, Air Force Institute of Technology (AU), Wright-Patterson AFB OH, March 2007.
28 Quaale, Ryan J., Ralph A. Anthenien, Joseph Zelina, and Jeffery Ehret, "Flow Measurments within a High Swirl Ultra Compact Combustor for Gas Turbine Engines," ISAVE-2003-1141, WPAFB, OH: 2003.
29 Zelina, J., G.J. Sturgess, and D.T. Shouse. "The Behaviour of an Ultra-Compact Combustor (UCC) Base on Centrifugally-Enhanced Turbulent Burning Rates," 40th AIAA/ASME/SAE/ASEE Joint Propulsion Conference and Exhibit, AIAA 2004-3541, Fort Lauderdale, FL: July 2004.
30 Eckbreth, A. C. In Gupta A. K., Lilley D. G. (Eds.), *Laser Diagnostics for Combustion Temperature and Species* (1st ed.). Tunbridge Wells, Kentucky: Abacus Press, 1998.
31 Spectra-Physics Lasers & Photonics. *Quanta-Ray Lab-Series Pulsed Nd:YAG Lasers User's Manual.* Mountain View, CA: 2001.
32 Cornelius. Tuneable Laser Diode Operations Manual, 2008.
33 Anderson, W. S. *Design, Construction, and Validation of the AFIT Small Scale Combustion Facility and Sectional Model of the Ultra-compact Combustor.* MS thesis, AFIT/GAE/ENY/07-M01. Graduate School of Engineering and Management, Air Force Institute of Technology (AU), Wright-Patterson AFB OH, March 2007.
34 Koether, S. J. *Validation of the AFIT Small Scale Combustion Facility and OH Laser-Induced Fluorescence of an Atmospheric Laminar Premixed Flame.* MS thesis, AFIT/GAE/ENY/07-S03. Graduate School of Engineering and Management, Air Force Institute of Technology (AU), Wright-Patterson AFB OH, September 2007.
35 (NASA RP-1311, 1996)
36 J. Luque and D. R. Crosley, "LIFBASE: Database and Spectral Simulation Program (Version 2.0.55)," SRI International Report MP 99-009, 1999.

Vita

Christina R Serianne graduate from Wayne High School in Huber Heights, Ohio. She enlisted in the Navy in 1994 and ended her active service obligation in 2002. She graduated from Embry-Riddle Aeronautical University in 2001with a Bachelors of Science in Professional Aeronautics.

She was an Aviation Electrician and Naval Aircrewman. She served on the P-3 Orion and C-9 Skytrain platforms. During her time in the Navy, she was stationed in VP-45 and VR-58 based in Jacksonville, Florida. She was awarded a DAGSI fellowship and entered the Graduate School of Engineering and Management; Air Force Institute of Technology. Upon graduation she will enter the doctoral program and pursue candidacy at the Air Force Institute of Technology.

REPORT DOCUMENTATION PAGE

Form Approved
OMB No. 0704–0188

1. REPORT DATE (DD–MM–YYYY)	2. REPORT TYPE	3. DATES COVERED *(From — To)*
26-03-2009	Master's Thesis	January 2006-December 2008

4. TITLE AND SUBTITLE

Tunable Diode Laser Absorption Spectroscopy Verification Analysis For Use In The Combustion Optimization And Analysis Laser Laboratory.

5a. CONTRACT NUMBER

5b. GRANT NUMBER

5c. PROGRAM ELEMENT NUMBER

6. AUTHOR(S)

Christina R. Serianne, Civilian

5d. PROJECT NUMBER

5e. TASK NUMBER

5f. WORK UNIT NUMBER

7. PERFORMING ORGANIZATION NAME(S) AND ADDRESS(ES)
Air Force Institute of Technology
Graduate School of Engineering and Management (AFIT/ENY)
2950 Hobson Way
WPAFB OH 45433-7765

8. PERFORMING ORGANIZATION REPORT NUMBER

AFIT/GAE/ENY/09-M17

9. SPONSORING / MONITORING AGENCY NAME(S) AND ADDRESS(ES)
Air Force Office of Scientific Research
Dr. Julian Tishkoff
4015 Wilson Boulevard
Room 713
Arlington, VA 22203-1954

10. SPONSOR/MONITOR'S ACRONYM(S)
AFOSR

11. SPONSOR/MONITOR'S REPORT NUMBER(S)

12. DISTRIBUTION / AVAILABILITY STATEMENT

APPROVED FOR PUBLIC RELEASE; DISTRIBUTION UNLIMITED.

13. SUPPLEMENTARY NOTES

14. ABSTRACT

The AFIT Combustion Optimization and Analysis Laser (COAL) laboratory has state-of-the-art laser diagnostic capability for combustion process. The research for this thesis served to enhance the COAL lab's capability. Currently, there are no known commercially available tunable diode lasers that produce Ultra-Violet radiation required for this analysis. Sum-frequency generation at 313.5 nm was utilized for high speed OH absorption and temperature measurements at a rate of 2kHz. The Tunable Diode Laser Absorption Spectroscopy system was validated by comparison with theoretical and well characterized experimental data by operating the system over a wide range of conditions for an H2 laminar flame produced by a Hencken burner. The TDLAS system was able to perform at reasonable accuracy. After validation, the system was also characterized for a turbulent environment by comparing turbulent and flame structure theory with results obtained from a C2H4/N2 jet flame. The testing was also conducted for a range of conditions and produced reasonable results.
The accuracy of the system is sufficient for utilization in investigating behavior in a turbulent, combusting environment.

15. SUBJECT TERMS
Combustion, Combustors, Experimental, Laboratory, Laser Diagnostics, Ultra-Compact Combustor, TDLAS, Hencken , turbulent jet flame, absorption spectroscopy

16. SECURITY CLASSIFICATION OF:			17. LIMITATION OF ABSTRACT	18. NUMBER OF PAGES	19a. NAME OF RESPONSIBLE PERSON
a. REPORT	b. ABSTRACT	c. THIS PAGE			LtCol Richard Branam, ENY
U	U	U	UU	125	19b. TELEPHONE NUMBER (Include Area Code) (937) 255-3636, ext 7485 e-mail: Richard.Branam@afit.edu